Movement artifacts in electrocardiography

Anni Pyysing

School of Electrical Engineering

Thesis submitted for examination for the degree of Master of Science in Technology.

Espoo 18.01.2018

Thesis supervisors:

Prof. Simo Särkkä

Thesis advisors:

D.Sc. (Tech.) Lauri Palva

M.Sc. (Tech.) Kimmo Suotsalo

Aalto University
School of Electrical
Engineering

AALTO UNIVERSITY
SCHOOL OF ELECTRICAL ENGINEERING

ABSTRACT OF THE
MASTER'S THESIS

Author: Anni Pyysing

Title: Movement artifacts in electrocardiography

Date: 18.01.2018 Language: English Number of pages: 7+74

Department of Electrical Engineering and Automation

Professorship: Sensor informatics and medical technology

Supervisor: Prof. Simo Särkkä

Advisors: D.Sc. (Tech.) Lauri Palva, M.Sc. (Tech.) Kimmo Suotsalo

Movement of the patient during electrocardiograph (ECG) recording is a severe source of artifacts. Recent technical developments have enabled ECG recording without continuous supervision by experts. However, ECG recording outside of hospitals is prone to poor quality and movement artifacts. Therefore, it is important to study how and how much ECG recordings are affected by movement.

Movement artifacts can hide signal components or mimic them, which causes false negative or false positive detections. Methods to manage movement artifacts include both computational and non-computational approaches. Computational approaches include, for example, adaptive filtering and machine learning methods. Additional variables that correlate with the artifact sources can be utilized in artifact recognition. For example, acceleration, impedance, and pressure signals have been studied as possible movement references. These additional signals are recorded by sensors that are placed on the ECG electrodes or on the patient's body.

In this thesis, the effect of movement artifacts is quantified using a simulation. The simulation makes use of open ECG databases. This study investigates how automated ECG analysis is affected by incremental increase in the movement artifact level. According to the results QRS detection statistics worsen with increased artifact levels.

Capturing a movement reference for ECG is studied by experimental research. ECG and inertial measurement unit signals were recorded during different movements in order to analyze the creation of movement artifacts and movement reference signals. According to the results, placement of the movement reference signal sensor has a significant effect on the results. Different movements are captured better by different sensors and affect different ECG leads with different strengths.

Keywords: electrocardiography, electrodes, signal processing, movement artifact, skin-electrode interface, artifact reduction, sensors

AALTO-YLIOPISTO
SÄHKÖTEKNIIKAN KORKEAKOULU

DIPLOMITYÖN
TIIVISTELMÄ

Tekijä: Anni Pyysing

Työn nimi: Liikeartefaktat elektrokardiografiassa

Päivämäärä: 18.01.2018 Kieli: Englanti Sivumäärä: 7+74

Sähkötekniikan ja automaation laitos

Professuuri: Sensori-informatiikka ja lääketieteellinen tekniikka

Työn valvoja: Prof. Simo Särkkä

Työn ohjaajat: TkT Lauri Palva, DI Kimmo Suotsalo

Potilaan liike sydänsähkökäyrämittauksen (EKG) aikana on merkittävä artefaktien lähde. Viimeaikainen teknologinen kehitys on mahdollistanut EKG-mittauksen ilman asiantuntijoiden jatkuvaa valvontaa. EKG-mittaukset sairaalaolosuhteiden ulkopuolella ovat kuitenkin erityisen alttiita huonolle signaalilaadulle ja liikeartefaktoille. Tämän vuoksi on tärkeää tutkia, miten ja kuinka paljon liike vaikuttaa EKG-mittauksiin.

Liikeartefaktat voivat joko peittää tai jäljitellä EKG-signaalin eri osia, aiheuttaen vääriä negatiivisia tai vääriä positiivisia havaintoja. Liikeartefaktojen vaikutusta voidaan vähentää sekä laskennallisten että muiden menetelmien avulla. Laskennallisia menetelmiä ovat esimerkiksi adaptiivinen suodatus ja koneoppimismenetelmät.

Artefaktojen lähteen kanssa korreloivia muuttujia mittaamalla voidaan edistää artefaktojen tunnistusta EKG-signaalista. Esimerkiksi kiihtyvyys-, impedanssi- ja painesignaalien käyttöä liikereferensseinä on tutkittu. Kyseisiä referenssisignaaleja voidaan mitata EKG-elektrodeihin tai potilaan kehoon kiinnitettävillä sensoreilla.

Liikeartefaktojen vaikutuksen suuruutta tutkitaan tässä työssä simulaation avulla. Simulaatiossa hyödynnetään avoimia EKG-tietokantoja. Tutkimuksessa tarkastellaan sitä, miten vähittäinen liikeartefaktatason kasvu vaikuttaa automaattiseen EKG-analyysiin. Tulosten mukaan QRS-detektioon liittyvät tilastot huononevat artefaktatason kasvaessa.

Liikereferenssin luomista tarkastellaan kokeellisen tutkimuksen avulla. EKG- ja inertiamittausyksikkö-signaaleja mitattiin erilaisten liikkeiden aikana, jotta voitaisiin havainnoida liikeartefaktojen ja liikesignaalin syntymistä. Tulosten mukaan liikereferenssiä mittaavan sensorin sijoituspaikalla on merkittävä vaikutus tuloksiin. Tietyt liikkeet saadaan paremmin mitattua eri tavoin sijoitettujen sensorien avulla. Lisäksi liikkeet vaikuttavat eri vahvuuksilla eri EKG-kytkentöihin.

Avainsanat: elektrokardiografia, elektrodit, signaalinkäsittely, liikeartefakta, iho-elektrodi rajapinta, artefaktien vähentäminen, sensorit

Preface

I would like to thank Aalto University and the department of Electrical Engineering and Automation for providing me with the opportunity to write my thesis in an inspiring environment. Specifically, I express my gratitude to my supervisor Prof. Simo Särkkä and advisors Dr. Lauri Palva and M.Sc. (Tech.) Kimmo Suotsalo for their valuable feedback. I would also like to express my appreciation to the team that conducted the experiments that were studied in this thesis, including Mr. Matti Suominen, Mr. Tuomas Lumikari, and Dr. Roland Hostettler.

Lastly, I want to thank my friends and family for their invaluable support during the thesis process.

Espoo, Otaniemi, 18.01.2018

Anni Pyysing

Contents

Symbols and abbreviations

Abbreviations

A-D	Analog-to-digital
AV	Atrioventricular
CPR	Cardiopulmonary resuscitation
CWT	Continuous wavelet transform
db6	Dauchebies wavelet 6
DSP	Digital signal processing
ECG	Electrocardiography
EDF	European data format
HMM	Hidden Markov model
HRV	Heart rate variability
ICA	Independent component analysis
IMU	Inertial measurement unit
LBBB	Left bundle branch block
LDA	Linear discriminant analysis
LMS	Least mean square
MI	Myocardial infarction, in other words a heart attack
MITDB	MIT-BIH arrhythmia database
NSTDB	MIT-BIH noise stress test database
PCA	Principal component analysis
PVC	Premature ventricular contraction
RBBB	Right bundle branch block
RLS	Recursive least square
RMS	Root mean square
SA	Sinoatrial
SNR	Signal-to-noise ratio
SQI	Signal quality index
STFT	Short-time Fourier transform

1 Introduction

Electrocardiography (ECG) is a common noninvasive method in medicine used to monitor and diagnose patients (Neuman, 2009b). ECG is a technique used to study the electrical activity of the patient's heart. Electrical activity of the heart can reveal substantial information about the patient's state if interpreted correctly (Thaler, 2015). The golden truth interpretations are made by experienced cardiologists. However, computational methods are increasingly capable of both preprocessing the signal for the cardiologist and producing an initial diagnosis (Martis et al., 2014).

Cardiologists make the diagnosis based on the graphical output of an ECG recording, called an electrocardiogram. A schematic of an ECG measurement setup and an electrocardiogram on the monitor are visualized in Figure 1. When the electric potential difference between two points is measured from the body surface, other signals than the signal of the heart are able to mix into the recording (Webster, 1984). These unwanted signals can be called either noise or artifacts, depending on the source. The terms noise and artifact are used in this thesis as described by Clifford (2006), "*artifact* is used to indicate the presence of a transient interruption (such as electrode motion) and *noise* is used to describe a persistent contaminant".

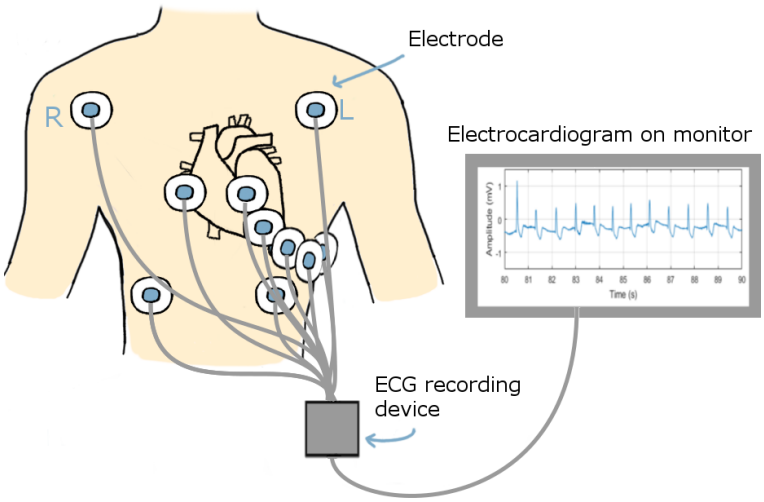

Figure 1: Schematic of an ECG recording setup that uses 10 electrodes.

There are several approaches to minimizing disturbances in the ECG. Various computational methods are used, ranging from simple filtering to more complex methods. Also, both the instrumentation and the measurement setup can be designed for this purpose (Neuman, 2009b).

Movement is one of the more difficult noise sources to exclude; the spectra of movement artifacts and the ECG signal itself overlap (Thakor et al., 1984). Furthermore, movement artifacts are dynamically changing (Raya and Sison, 2002). The importance of understanding the exact effect of artifacts on ECG is becoming more important as the medical field develops. The development of ECG is discussed in Section 2.1.

The first goal of this thesis is to estimate how movement affects the reliability of computational cardiology methods. The research questions related to this goal include:

- How do the movement artifacts affect computational analysis?
- Are different beat types affected similarly by movement artifacts?

Three algorithms are used to process ECG data with and without artifacts in order to quantify the effect of movement on computational ECG interpretation.

The second goal of this thesis is to evaluate measurement setups that are used to assess ECG movement artifact sources. This part has two secondary objectives. The first is to gather knowledge on methods that have been applied previously. The second is to assess the effect of sensor placement via experimental research. Design and implementation of the experimental research is conducted by the research group in which the author is writing the thesis. The research questions related to the second goal include:

- How have additional sensors been applied in movement artifact reduction?
- How are different movements captured by different sensors?
- What is the ideal setup for the movement measurement?

The subject of this thesis is focused on, but not limited to, reducing artifacts by methods that utilize movement recordings. However, the field of electrocardiography is discussed more widely to give the topic necessary context. The background review in Chapter 2 begins with a general view of the development and principles of ECG, gradually narrowing down to the most relevant themes to the goals of this thesis. Methodological choices of the thesis project and the research process are discussed in Chapter 3. The thesis process consists of both literature research in the form of background review and data based studies. The data used in this thesis process is partly from an open access database and partly from the experiments conducted at Aalto University. Results from both simulation and experimental studies are given in Chapter 4. Evaluation and reflection of the results is conducted in Chapter 5. Finally, a brief overview of the topics and results of the thesis is provided in Chapter 6.

2 Background

The following sections cover the development of ECG, the most important components of the ECG signal, the main aspects of signal processing, disturbances in ECG, and methods to reduce artifacts. The last background sections focus on literature that is most relevant to the research questions and goals of the thesis. First the history of electrocardiography is discussed shortly to give the reader a view into the development preceding the invention of the standard 12–lead ECG.

2.1 History and development of electrocardiography

The effects of electricity on animals and different materials have been observed since the ancient times, according to Geddes and Hoff (1971). However, the history of bioelectricity began with the discovery of animal electricity by Luigi Galvani in the 1780's (Burch and DePasquale, 1990).

The first human electrocardiogram was recorded in 1887 by Augustus D. Waller using a mercury capillary electrometer with surface electrodes on the chest (Lüderitz, 2003). However, the next year Waller used buckets of salt water in which the patients extremities were immersed (Lüderitz, 2003). Over the following years after Waller's experiments, the familiar P-QRS-T waveform was discovered and recorded by Willem Einthoven (Burch and DePasquale, 1990). Einthoven was also able to develop a string galvanometer that had excellent performance, which eventually led to the wider application of the ECG as a clinical tool (Barold, 2003). Einthoven is also known as the developer of the standard limb leads I, II, and III, later called the Einthoven's triangle (Burch and DePasquale, 1990). However, nowadays the buckets of salt water are approximated by electrodes (Goy et al., 2013), which are discussed in the next section.

In the early years after the development of ECG, the clinical significance was further advanced by Sir Thomas Lewis, who was able to study many disorders of the heart with ECG, followed by Frank Wilson, who developed the concept of Wilson's central terminal and the unipolar chest leads (Barold, 2003). Even though it was possible to examine arrhythmias already with the three-lead ECG, there was still much uncovered area in the heart. Consequently, more leads were developed for standard use, to be able to diagnose, for example, myocardial infarctions. The chest leads were standardized and named V1-V6 in 1938. The standard 12-lead electrocardiogram was established in 1954 after the invention of the three augmented unipolar limb leads a-VL, a-VR and a-VF that allow yet more specific detection of the heart's electrical signal (AlGhatrif and Lindsay, 2011). Standardization of the leads was published by the American Heart Association (1967).

These days ECG is commonly used to diagnose and monitor patients in hospitals. However, remote healthcare is getting more common. Biomedical signals might be recorded by the patients at their homes without assistance from a medical professional. As ECG is one of the most commonly measured signals, it is natural that systems that can be reliably utilized by non-professionals should be developed. Single-lead ECG devices are typically applied in remote healthcare due to ease of use, which

limits the methods that can be applied for signal quality enhancement (Redmond et al., 2012). It has also been suggested that multimodal sensor systems will be increasingly applied in remote healthcare. Multimodal systems integrate signals from various sensors, such as ECG, pulse oximeter, and inertial sensors (Redmond et al., 2012).

Additionally, wearable and wireless ECG methods are increasing as continuous health monitoring of vital signs is emerging. Research on these topics is focused especially on the elderly and the methods are applied in care facilities (Baig et al., 2013). Remote monitoring of vital signs might also utilize mobile devices, and sensors could be managed via a smart phone. However, system stability is typically lower compared to other devices due to problems in connectivity, transmission speed, and battery life (Baig et al., 2013).

Patient-made recordings are prone to errors, poor signal quality, and artifacts. Therefore, the ability to detect poor quality signals and derive an accurate diagnosis based on noisy signals is especially important. Both signal quality detection and signal quality enhancement methods should be developed in response to the increase in patient-performed measurements.

2.2 Physiology and electrical conduction of the heart

In this section, physiology of the heart is described briefly in order to understand the origin of ECG. For more detailed explanation of the physiology and anatomy of the heart one can refer to the textbooks by Khurana (2005) and Ward and Linden (2013), which are referenced in this section.

The heart is a system of two pumps in series that drives blood flow. Blood distributes vital elements to the cells in the entire body and moves waste to the correct organs. Oxygen rich blood is pumped from the heart into the body and oxygen poor blood returns to the heart from the body full of CO_2. The importance of the correct functioning of the heart is clear as one recalls that all human cells require oxygen in order to function – oxygen is vital in the reactions that cells utilize to gain energy. Without energy, the cells will quickly begin to die. The first organ to lose its function in the case of oxygen deprivation is the brain, as the brain cells can only survive minutes without oxygen supply.

The heart consists of two halves, both of which have an atrium and a ventricle. The blood enters the heart through the right atrium and travels to the right ventricle, from which it is pumped into the lungs. Oxygenated blood enters the heart again and passes through the left atrium and continues into the left ventricle. The left ventricle must pump the now oxygenated blood outside of the heart to be utilized by the cells of the entire body. One-directional blood flow from the atria into the ventricles to the parts outside of the heart is ensured by valves that open and close by the force of the blood flow. A diagram of the heart can be found in Figure 2.

The heart walls have thick layers of cardiac muscle, which consist of cardiac muscle cells. All cells have a membrane separating them from their environment. The cell membrane acts as a selective barrier controlling, for example, the intake and output of charged K^+ ions (Ward and Linden, 2013, pp. 20–21). The resting cell

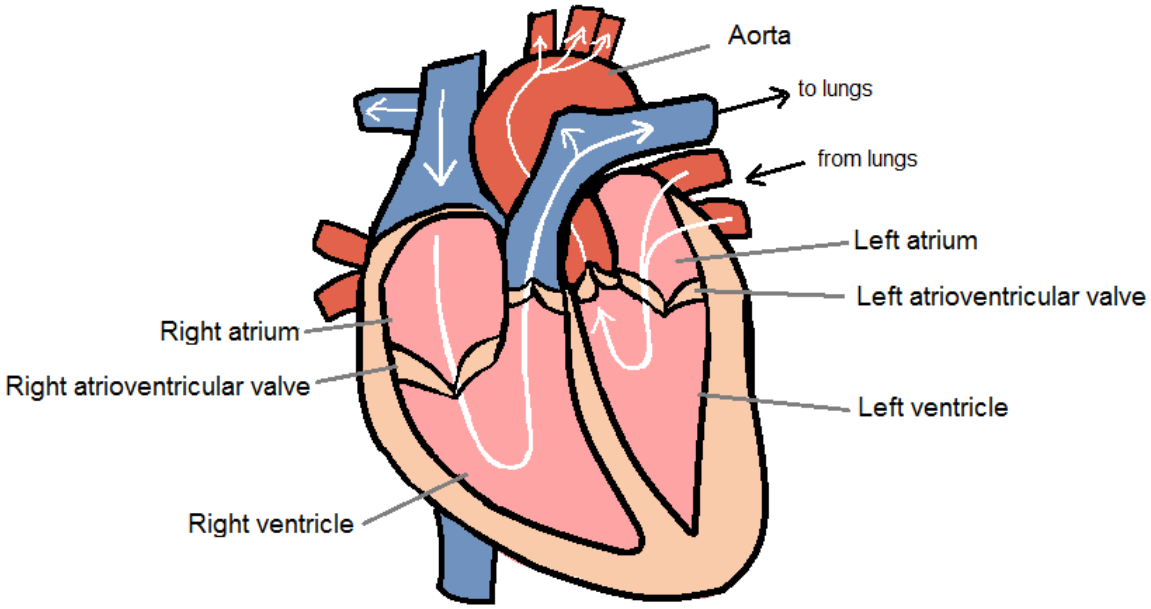

Figure 2: The human heart. Direction of blood flow is marked by arrows. Vessels that carry oxygen rich blood are red and vessels that carry oxygen poor blood are blue in the figure.

membrane is able to maintain a concentration difference across the cell membrane, which is in balance with the resulting potential difference. Therefore, all cells have a resting potential, namely a potential difference between the inside and outside of the cell. The inactive electrical state of the cells is called the resting membrane potential. The resting membrane potential is around -90 mV in the heart (Ward and Linden, 2013, p. 49), which means that the inside of the cells is more negative than the outside of the cells.

Excitable cells can be triggered by external signals and depolarize (Ward and Linden, 2013, p. 23). Depolarization means that the cell membrane becomes temporarily less polarized, in other words, less negative. However, the cell will not stay depolarized, and will quickly return to its resting potential. This phase is called repolarization. The cardiac muscle is excitable and responds to stimulation by depolarization, which is followed by contraction. Organized contraction of the muscle is normally controlled by its main pacemaker, the sinoatrial (SA) node. The heart has specialized pacemakers that act as the origin of cardiac impulses, which are conducted via a conduction system visualized in Figure 3.

Cardiac muscle fibers have gap junctions that act as low resistance bridges and allow the depolarization wave to spread in the muscle (Khurana, 2005). Therefore, the cardiac muscle acts as a functional syncytium, that is, cells that behave as one large cell, but in fact are separate. Correct electrical synchronization of the heart muscle is vital to its function. The cardiac muscle cells must depolarize and subsequently contract in coordination to produce a strong contraction that is able to

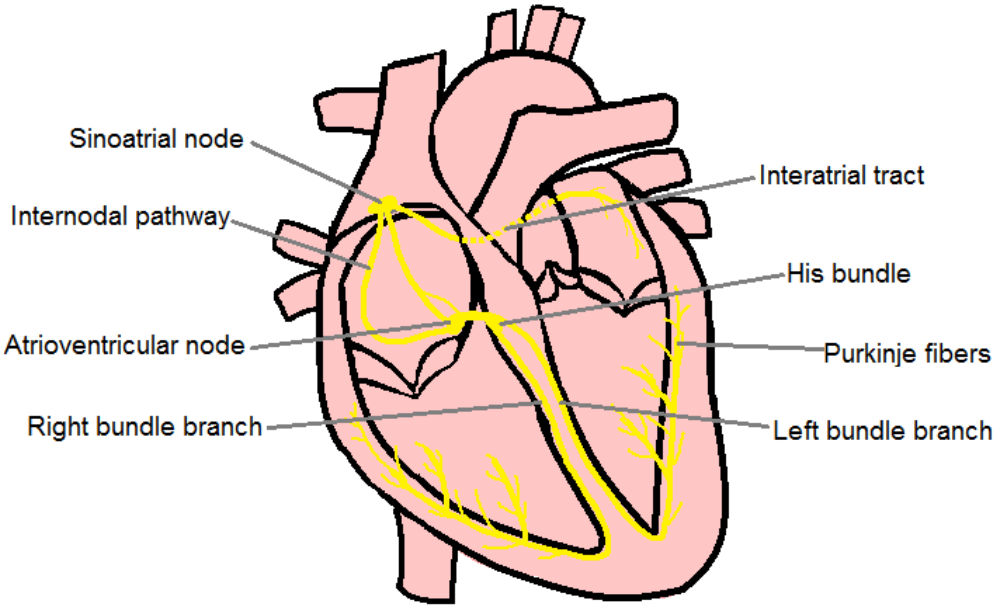

Figure 3: Electrical conduction in the human heart follows a specific route that begins in the sinoatrial node.

push the blood through the valves.

Electrical activation of the heart originates from the SA node in the right atrium. The activity of the SA node defines the heart rate. The operation of the SA node is affected by specific transmitters. Through these transmitters, the SA node is able to get input from the other parts of the body (Ward and Linden, 2013). The transmitters that tune the function of the SA node are released based on the person's activities. For example, a transmitter that rises the heart rate called noradrenaline is released under physical activity.

The depolarization wave travels from the SA node to the atria and the following conduction tracts that can be seen in Figure 3. The two atria contract simultaneously due to the fast conduction speed of the interatrial tract. The impulse travels from the SA node into the atrioventricular node. The impulse descends towards the ventricles via the bundle of His, which divides into the left and the right bundle branch. The bundle branches divide into Purkinje fibers and the signal spreads up the outer walls of the ventricles (Khurana, 2005).

2.3 Principles of electrocardiography

This subsection covers the principles of electrocardiography including an overview of ECG instrumentation and some diagnostic aspects. Electrocardiography is based on detecting changes in the electrical potential which arise due to the electrical activity of the heart (Neuman, 2009a). Duration, frequency, amplitude, and direction of the depolarization and repolarization waves reveal information about the heart's

functioning (Khurana, 2005, Chapter 15). Changes in the electrical potential can be detected on the body surface, which makes ECG measurements noninvasive and easy to conduct. ECG can be used in, for example, initial diagnosis of the patient, which might be followed by more invasive methods such as angiography.

There are at least three common ECG measurement types that are applied for specific purposes, such as monitoring or diagnosis. ECG is typically recorded using a standard 12-lead ECG setup or a Holter (ambulatory ECG), both of which have their advantages and disadvantages (Jabaudon et al., 2004). The standard ECG is recorded while the patient is lying on his or her back and is therefore called the resting ECG. The electrode setup and the leads of 12-lead ECG are discussed in more detail in the following chapter. Stress ECG is recorded while the patient is either walking or cycling. Stress ECG can be utilized to assess heart related abnormalities that can only be found in the ECG during exercise. It can be used to detect coronary artery disease and to estimate the exercise capacity of people with cardiac abnormalities (Lear et al., 1999).

Rest and stress ECGs are typically recorded in hospital settings, but ECG can also be recorded in other locations. Ambulatory ECG means that the patient is allowed to leave the hospital and perform normal activities during the ECG measurement. Ambulatory ECG devices can be used to monitor the patient's heart for several days (Jabaudon et al., 2004). This method can reveal heart conditions that would not be found during an ECG measurement in the hospital, since some heart problems occur only rarely or during certain activities. Ambulatory ECG can be performed using a Holter monitor, which is called Holter monitoring. Holter monitors record typically only two or three channels.

2.3.1 Standard 12-lead ECG

The ECG signal is measured using electrodes attached to different points on the patient's body (Neuman, 2009a). Leads are derived from the electrical potentials measured by the electrodes, and each lead sees the heart from a different angle. The standard 12-lead ECG is recorded using 10 electrodes that comprise three limb leads, three augmented limb leads, and six chest leads. Summary of the standard 12-lead ECG is given in Table 1 and placement of the electrodes is visualized in Figures 4 and 5.

Bipolar leads measure the electric potential difference between two electrodes, and unipolar leads measure the voltage between an electrode and the Wilson's central terminal (Wilson et al., 1934). The Wilson's central terminal is constructed by connecting the electrodes on the right arm (R), the left arm (L), and the left leg (F) (Katz, 2010). It is defined as the approximation of a zero reference electrode for the unipolar ECG leads (Okamoto and Mashima, 1998). However, the augmented limb leads that complement the limb leads are actually connected to modified versions of the Wilson's central terminal (Neuman, 2009a, pp. 247–248). The chest leads record the potential differences between the six electrodes placed on the chest and the Wilson's central terminal, and the limb leads are based on the electodes placed closest to the limbs.

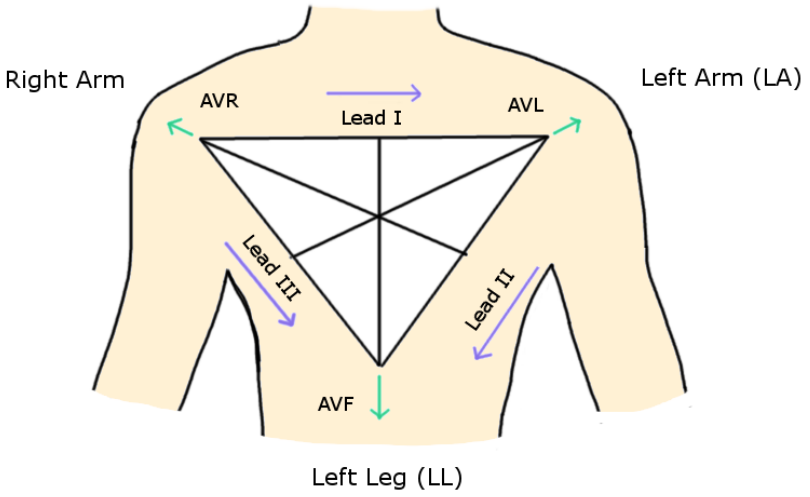

Figure 4: Einthoven's triangle is composed of the bipolar limb leads I-III in the coronal plane. The augmented limb leads aVL, aVR, and aVF are placed between the limb leads. Directions of the leads are marked by arrows.

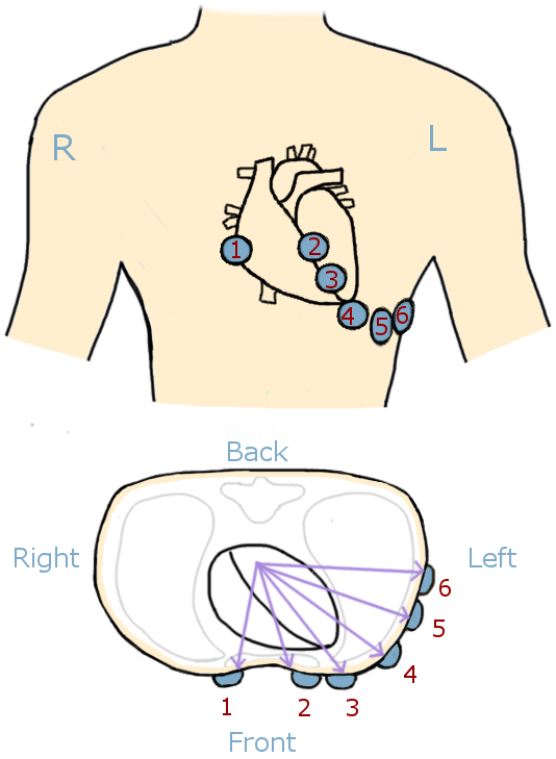

Figure 5: Placement of the chest electrodes in the coronal plane (top) and in the transverse plane (bottom). The electrodes that are used to construct the chest leads V_1-V_6 are marked by numbers 1-6. Directions of the corresponding leads are marked by arrows.

Table 1: The standard 12 leads are based on 10 electrodes placed on different parts of the body surface. Each lead is based on either the potential difference between two electrodes, one of which is the reference, or one electrode and the V. V is the original Wilson's central terminal for the chest leads and the modified version for the augmented limb leads. The table was adapted from the book by Katz (2010, pp. 420–423).

Lead type	Lead name	Angle*	Electrode	Reference
Limb leads	I	0°	Left arm	Right arm
	II	60°	Left leg	Right arm
	III	120°	Left leg	Left arm
Augmented limb leads	aVR	-150°	Right arm	V
	aVL	-30°	Left arm	V
	aVF	90°	Left leg	V
Chest leads	V_1	100°	Right of sternum	V
	V_2	80°	Left of sternum	V
	V_3	75°	Left of V_2	V
	V_4	60°	Left of V_3	V
	V_5	30°	Left of V_4	V
	V_6	0°	Left of V_5	V

* Angles are on the coronal plane for the limb leads and the augmented limb leads, and on the transverse plane for the chest leads.

2.3.2 The skin-electrode interface

The properties of the skin-electrode interface depend on both the electrodes and the skin. Detailed descriptions of the electrodes (Neuman, 2009b) and the skin (Moreau et al., 2002, Chapter 3) can be found in the literature. This section provides a simplified description of the interface.

The most common electrodes currently used in ECG recording are silver/silver-chloride (Ag/AgCl) electrodes (Neuman, 2009b). They are attached to the skin via self-adhesive pads. A single electrode consists of a silver core that is coated with a thin layer of silver chloride (AgCl) that is slightly soluble. Electrolyte gel is placed between the electrode and the skin in order to couple the electrode to the skin. The electrolyte gel that contains Cl^- ions is highly conductive and transfers the potential changes from the skin's surface to the electrode. More specifically, the ion current in the skin and the electrolyte is transformed into electron current in the lead wires at the gel-electrode interface.

The electrolyte gel-skin interface has a good electrical contact due to the Cl^- ions (Neuman, 2009b). However, the electrical properties of this contact are affected by the skin's condition. Skin preparation is necessary before the ECG recording since hair, dead skin, dirt, sweat, oil, and chemicals affect the skin's impedance and the

electrode's distance from the skin (Crawford and Doherty, 2011, pp. 33–36). Possible skin preparation steps include hair removal, washing by soap, and light abrasion.

Skin consists of two main layers, the epidermis and the dermis (Moreau et al., 2002, Chapter 3). The uppermost layer of the epidermis is called stratum corneum. Dermis lies below the epidermis and is connected to subcutaneous tissue that consists mainly of fat cells and is not a part of the skin. The surface of the skin is not similar in all people, and the consistency of the skin varies between different body parts. Especially the thickness of stratum corneum varies (Holbrook and Odland, 1974). It consists of keratin based dead cells and has different electrical properties from the rest of the skin.

The effect of each skin layer to the properties of the skin-electrode interface is visualized in Figure 6. The equivalent circuit of the skin-electrode interface is displayed as it was presented by Neuman (2009b). Stratum corneum is the main source of the skin potential (Tam and Webster, 1977) and the potential difference across the interface is represented by a voltage source in the circuit diagram. Epidermis can be modeled as a parallel RC circuit and the deeper layers of the skin act as a resistor. Therefore, the electrical properties of the skin become more stable when the stratum corneum is removed, even though it is able to regenerate during longer measurements. Stratum corneum is constantly worn off and replaced by new dying cells from below.

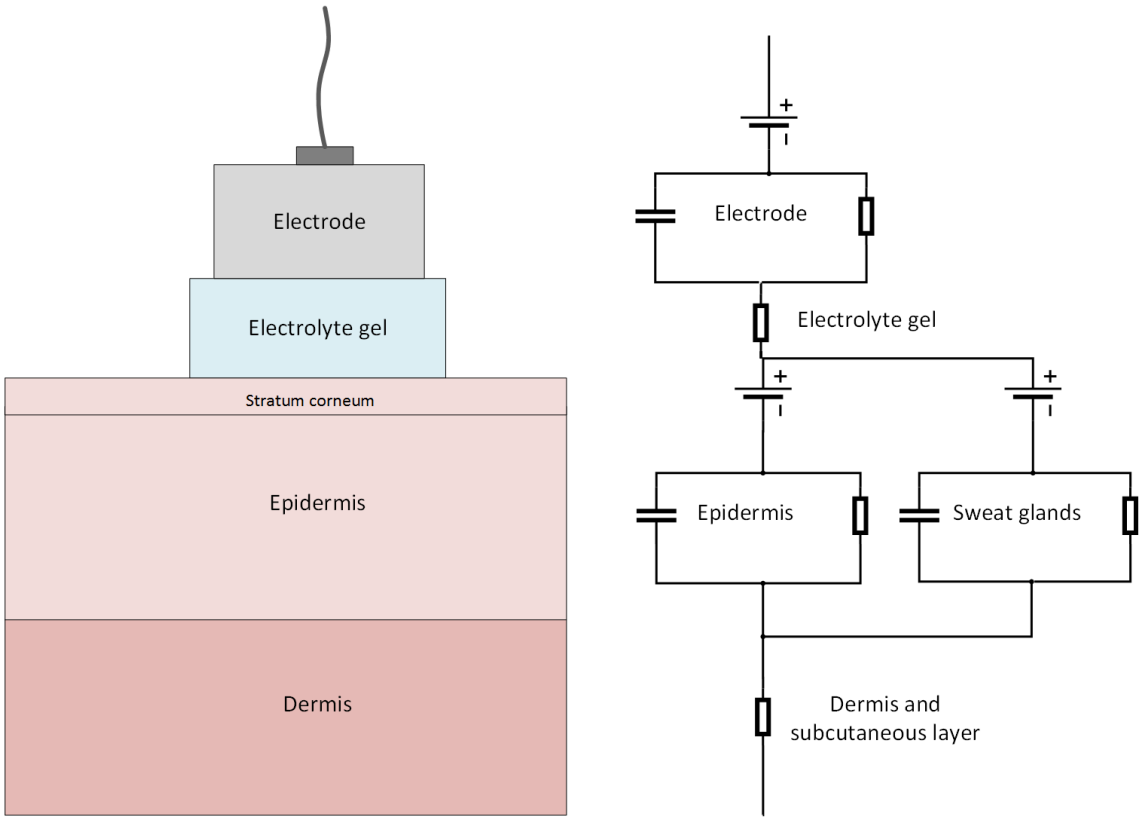

Figure 6: Skin-electrode interface can be modeled as an electric circuit, as presented by Neuman (2009b).

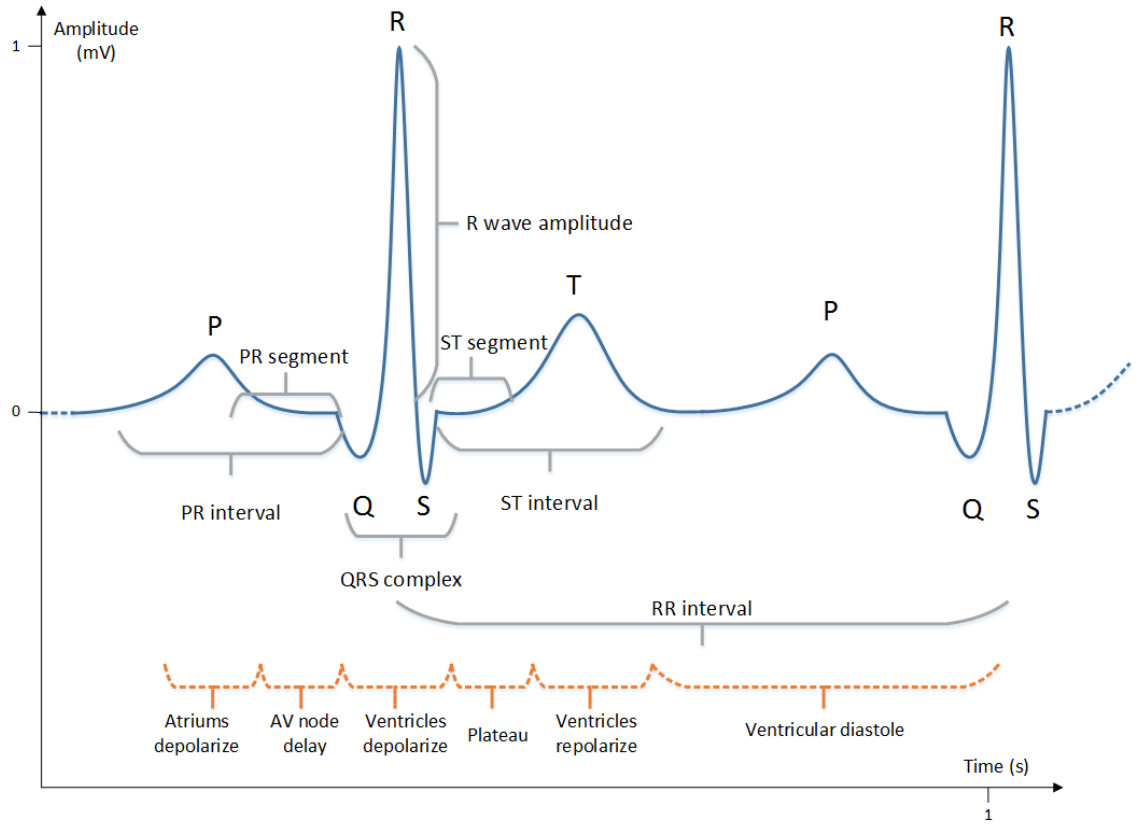

Figure 7: Two heart beats on the typical ECG signal. The P, Q, R, S, and T waves are marked by letters. Approximate intervals and segments are marked by horizontal brackets. Electrical phenomena corresponding to the ECG signal are marked by horizontal orange dashed brackets. More details about the different sections in the ECG signal can be found in the book by Katz (2010).

2.3.3 Structure of the ECG signal

The structure of the ECG signal is connected to the electrical conduction in the heart, which was discussed in Section 2.2. Detailed description of the origin of the ECG signal, and how it is related to the ECG waveform can be found in the book by Katz (2010, Chapter 15). Next, a short summary of the topics is provided.

Depolarization and repolarization waves in the heart muscle are seen as voltage changes in the ECG leads. Each lead sees the waves differently, since they are placed in different angles with respect to the heart (Katz, 2010). A visualization of a typical heart beat recorded on the ECG is given in Figure 7.

Activation of the SA node is not seen in the ECG using normal surface electrodes (Katz, 2010). Therefore, the ECG signal begins with the next event, atrial depolarization. Atrial depolarization creates the P wave, which is followed by the QRS complex and the T wave. The most recognizable points in the ECG signal are the R peaks, which have the highest amplitude. The other waves in the QRS complex, namely Q and S, might not always be separated in the ECG. The main

Table 2: The main features of an ECG signal that consists of repetitive patterns labeled P and T waves and the QRS complex. A detailed description of the relation between impulse propagation through the heart and the waves, intervals and segments in the electrocardiograph can be found in the book by Katz (2010).

Type	Name	Origin
Wave	P	Atrial depolarization
	Q	Depolarization of the interventricular septum, area between the ventricles
	R	Depolarization of the main mass of the ventricles
	S	Final depolarization of the ventricles, up the outer walls
	T	Repolarization of the ventricles
Section	QRS complex	Ventricular depolarization
	RR Interval	Time between consecutive R-peaks; inverse of the heart rate
	PQ Interval	Duration of AV conduction; from AV node to His-Purkinje fibers
	QT Interval	Ventricular action potential
	ST Segment	Plateau; ventricles fully depolarized

characteristics of an ECG signal and their origin are summarized in Table 2.

An upright wave is recorded on a chest electrode when a wave of depolarization travels towards the Wilson's central terminal. The strong depolarization of the left ventricle dominates the signal recorded by the chest electrodes and can hide the depolarization of the right ventricle. The direction of the first depolarication wave, that corresponds to ventricular activation, is to the left, as can be deduced from Figure 3. Therefore, depolarization of the left ventricle is seen as a strong positive peak on leads V_5-V_6 as their exploring electrodes are placed to the left of the heart and Wilson's central terminal (Katz, 2010). However, simultaneous depolarization of the right ventricle is not seen as a positive peak on leads V_1-V_2 because it is overpowered by the effect of left ventricular depolarization. Therefore, the QRS complex seems inverted on the first chest leads placed in front of the right ventricle

that see the depolarization wave moving away from their exploring electrodes. A *transitional QRS* is typically seen in leads V_3-V_4 where the upward and downward deflections are nearly equal.

2.3.4 Sinus rhythm and arrhythmias

It is possible to get a large amount of information about the condition of the heart based on an ECG recording. Reliable diagnosis would require years of expertise and is usually done by a skilled cardiologist. Detailed ECG diagnosis is out of the scope of this thesis and one can refer to the book by Thaler (2015) for detailed description of ECG analysis. However, common signs of heart related abnormalities are discussed in this chapter as a basis for separating heart-related issues from ECG signal quality complications.

The normal sinus rhythm is seen in Figure 7 and the most important waves and signal segments are named in Table 2. Abnormalities in the ECG wave can be used in diagnosing a patient with heart-related symptoms and discovering potential risk factors in seemingly healthy patients. For example, unusually long intervals can indicate conduction problems in the underlying area. Although the ECG patterns vary even between healthy individuals, generalizations can be made to differentiate normal and abnormal ECG signal patterns. Some important diagnostic markers in the ECG include peak amplitude, peak shape and width, missing peaks or extra peaks, length of peak intervals, and the heart rhythm. Diagnosis of heart diseases is a complex process based on multiple factors, yet some simplified examples are provided next. More details can be found in the textbook by Goy et al. (2013), which was used as the main reference for this chapter.

Unusually long PR intervals (>200 ms) are a sign of delayed conduction in the atrium, AV node and His bundle (Goy et al., 2013). This is called a first degree AV block. Different types of second degree AV blocks include progressive PR interval length and blocked P waves, which are P waves not followed by a QRS complex. Complete disruption of AV conduction will cause the atria and the ventricles to have independent rhythms and the P waves will occur more frequently than the QRS complexes. AV blocks can be caused by a myocardial infarction that has caused a failure of AV nodal cells or the His-Purkinje system, drugs that block the AV-node, or a degenerative disease of the conduction system. A more specific location of the block can be based on QRS complex morphology, which might help in the planning of treatment.

Unusually wide QRS complexes (>120 ms) are a sign of conduction disturbance in the ventricles (Goy et al., 2013). If conduction in the right and left bundle branches is compromized, depolarization spreads via the ventricular muscles instead, which is slower. Block of conduction in the left bundle branch is called a left bundle branch block (LBBB) and block of conduction in the right bundle branch is called a right bundle branch block (RBBB). LBBB and RBBB can be separated based on the shape of the QRS complex. As the conduction in LBBB and RBBB will have a different directionality, the diagnosis is based on signals from multiple ECG leads.

Changes in the baseline of the ST segment are called ST segment deviation. ST

elevation and depression are important diagnostic markers for myocardial infarction. They are used, for example, to estimate MI severity and to decide the best treatment plan (Schröder et al., 2001).

Irregular heart beats, in other words, cardiac arrhythmias are classified into bradycardia, premature beats, and tachycardia. Bradycardia means an abnormally slow heart rate, whereas tachycardia is a series of premature beats that result in a rapid heart rate. Ventricular tachycardia might be followed by ventricular flutter, which in turn can turn into ventricular fibrillation, which is a very dangerous condition (Ma et al., 2009). An example of ventricular tachycardia and ventricular flutter is found in figure 8, where it can be seen that the flutter wave is substantially different from the sinus rhythm. Arrhythmias originate from several mechanisms, one of which is re-entry of the electrical impulse. Re-entry means that the electrical impulse travels in the heart muscle in a circular manner, which can cause tachycardia (Antzelevitch and Burashnikov, 2011).

Another mechanism behind cardiac arrhythmia is abnormal impulse formation (Antzelevitch and Burashnikov, 2011). Disturbance of the heart's main pacemaker, the SA node, might result either from failure to produce an impulse or to conduct the impulse further. Sino-atrial disturbances might be impossible to diagnose based on a normal surface ECG since activation of the SA node is only seen by intracardiac electrodes placed near the SA node. However, abnormalities in the PP interval can be a sign of sino-atrial disturbance. The PP interval is the time between consecutive P waves. A third degree SA block will cause the heart beat to be slower than usual. Unusually fast SA node activation is called sinus tachycardia (Katz, 2010).

Another part of the conduction system that is capable of working as a pacemaker can take over the rhythm if SA node stops working for a longer period. Rhythm produced outside of the SA node is called an escape rhythm. An escape rhythm might be apparent as missing P waves. However, a rhythm initiated outside of the SA node can also be faster than usual, in which case it is called junctional tachycardia (Katz, 2010).

Both late and early beats indicate that the depolarization wave was initiated outside of the SA node. Longer than expected RR interval (late beat) means that the activity originated in another pacemaker than the SA node. Shorter than expected RR interval (early beat) indicates a premature ectopic beat. Premature ectopic beats originated above the ventricles are called supraventricular extrasystoles.

An example of ECG signal that begins with ventricular tachycardia that progresses into ventricular flutter is given in Figure 8. Both rows include premature beats that arise from the ventricles called premature ventricular contraction (PVC), which are relatively common even in healthy hearts. However, more than two successive premature beats that cause the rhythm to deviate from normal is tachycardia. The PVCs in the second row are early compared to the normal rhythm and followed by a compensatory pause.

Installing an artificial pacemaker is one option used to treat arrhythmias (Zipes et al., 1968). Arrhythmias are detected using algorithms that control the artificial pacing. Arrhythmia detection algorithms used with the pacemakers are specifically tuned for each case (Jean-Jacques et al., 2004). An artificial pacemaker is used to

aid the patient's heart to produce an adequate heart rate. A pacemaker might be needed because of a slowly functioning natural pacemaker or a block in the heart's electrical conduction system. A beat initiated by an artificial pacemaker instead of the heart's pacemaker cells will cause abnormal peaks and wave shapes in the ECG record. Artificial pacemaker spikes on the ECG can be seen in Figure 9.

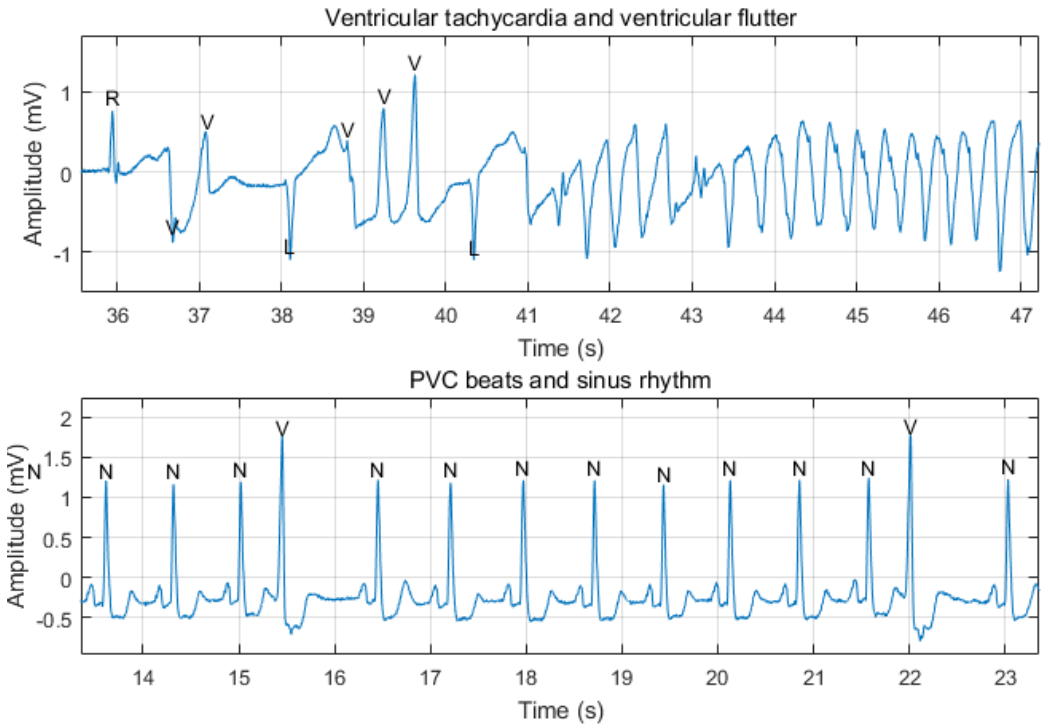

Figure 8: Ventricular tachycardia changing to ventricular flutter in the ECG recording 207 from MITDB (top) is compared to sinus rhythm that contains two PVCs in MITDB record 105 (bottom). PVCs are marked by V and normal beats are marked by N. The record 207 (top) includes also two LBBB beats, which are marked by L.

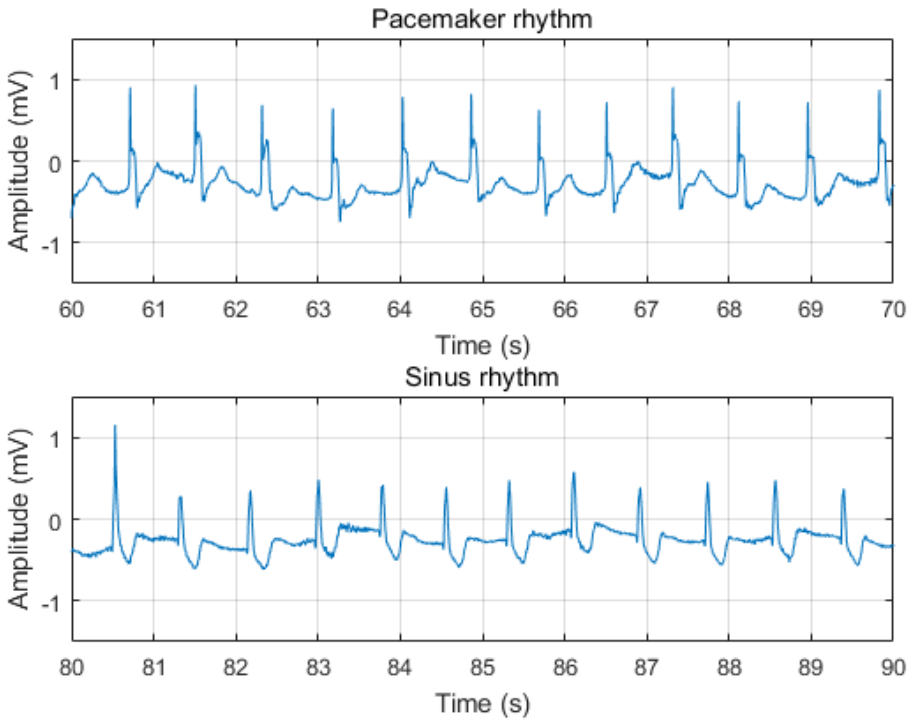

Figure 9: Pacemaker rhythm (top) compared to sinus rhythm (bottom) that is initiated by the SA node in MITDB record 102.

2.4 ECG signal processing

ECG signal processing makes use of the same methods as other biomedical signal processing areas. For a broad review of the most important methods in biomedical signal processing, the reader can refer to textbooks, such as the one by Rangayyan (2002). The following sections are mainly based on the book by Semmlow (2009).

ECG signal processing can be divided into analog and digital signal processing (DSP). Analog signal processing involves amplification and filtering, but most signal processing is typically done in digital format. The analog signal must also be converted to digital prior to DSP. Digital signal processing consists of several steps, but the exact number of steps depends on the implementation.

2.4.1 Signal conversion

Electrical potentials in the heart are converted into electrical signals using electrodes and amplifiers, which capture an analog signal. ECG electrodes were discussed in Section 2.3.2. Criteria for the selection of electrodes include high sensitivity and specificity in addition to low noise, although virtually all electrodes produce some noise. Environmental noise, electronic noise, and signal artifacts can be reduced by electrode design. The aim of electrode design and many digital signal processing methods is to achieve a higher signal-to-noise ratio, in other words, to identify the waveform of interest from all other parts of the signal (Semmlow, 2009). Signal-to-noise ratio is calculated in decibels according to Equation (1), which is

$$\mathrm{SNR_{dB}} = 10 \log_{10} \left(\frac{P_{\mathrm{signal}}}{P_{\mathrm{noise}}} \right). \tag{1}$$

Analog filters are required before the signal is digitized, because the signal must not contain frequencies that are higher than half of the sampling frequency according to Nyquist–Shannon sampling theorem. If higher frequencies were present in the signal, they would cause artifacts at lower frequencies. This phenomenon is called aliasing. Analog low pass filtering is conducted by an electronic device prior to digitization. Antialiasing filters are necessary already before digitization since aliasing cannot be determined from the sampled data points (Bates, 2012).

An analog-to-digital converter is used to digitize the signal and the signal is either stored before further processing or processed immediately if the system is a real-time application. Analog-to-digital conversion means converting the measured voltage into a digital number. Because the voltage changes in the heart are continuous in both time and amplitude, the signal must be sliced/sampled in both time and amplitude to be stored in digital format. Resolution of the A-D conversion is given as the number of bits in the binary output, which is usually 8, 12, or 16. The minimum resolvable voltage step q is calculated as $q = {}^{V_{max}}/_{2^N}$, where V_{max} is the positive voltage range and N is the number of bits (Semmlow, 2009, pp. 20–21).

The noise produced by converting the continuous signal into non-continuous or the quantization is called quantization error. Despite the quantization error it is not

reasonable to increase the number of bits in the A-D conversion because of other noise that will nevertheless decrease the SNR (Semmlow, 2009).

2.4.2 Digital ECG processing steps

The first computer processing methods for ECG focused on mimicking the actions of cardiologist by applying rules in a decision tree like manner. Nowadays, computerized methods are diverse and the methods applied are designed specifically for the application environment; for example, processing the stress ECG and the rest ECG are highly different (Sörnmo and Laguna, 2005). However, most of the DSP algorithms consist of similar basic blocks. The most common blocks of DSP systems are given in Figure 10.

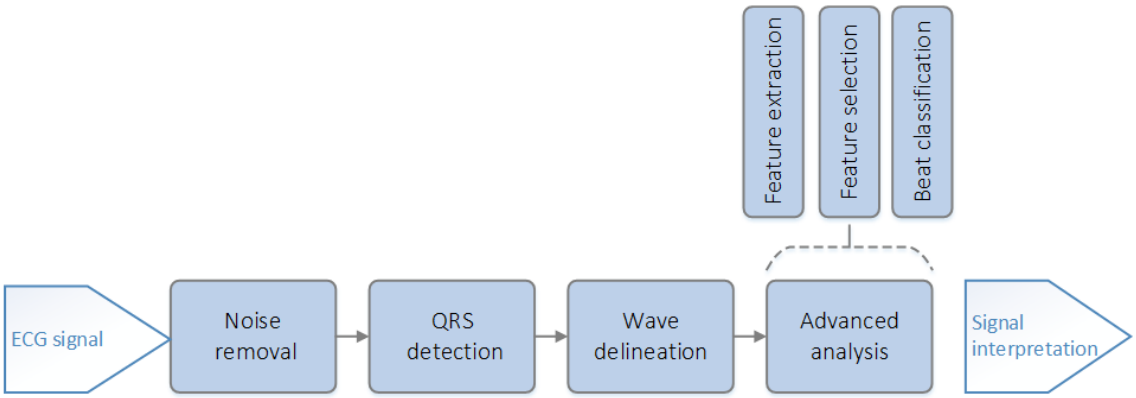

Figure 10: Common blocks of digital ECG signal processing.

Noise removal is necessary before applying methods that make interpretations about the ECG signal. Several types of noise and artifacts can be present in the ECG recording regardless of the analog filtering conducted prior to A-D conversion. Bandpass filters and ensemble averaging are examples of digital noise removal methods applied in ECG signal processing (Sörnmo and Laguna, 2005). Artifacts and noise are discussed in more detail in Subsection 2.5.

Digital filters are based on separating the frequency bands of the noise or artifacts and the signal. However, the spectra of the disturbances and the signal typically overlap. Therefore, filtering might remove components from the heart's signal in addition to removing the noise. For example, removing the powerline signal at 50 Hz using a band-reject filter will remove the 50 Hz signal components from the signal of interest as well. Losing the original waveform of the signal of interest due to filtering is called distortion. However, some components of the heart's signal can also be purposefully removed in signal preprocessing. Signal preprocessing often involves a high-pass filter that attenuates not only the noise but also the P wave and the T wave prior to QRS-detection (Kohler et al., 2002).

Averaging is another method to reduce noise in signal processing. It is a powerful method if multiple observations of the signal are available from multiple sensors (Semmlow, 2009). Another option is so called ensemble averaging. For example,

ensemble averaging over the QRS complexes will provide the average waveform, instead of a simple time average.

QRS-detection is the first step after noise removal. The QRS complex and specifically the R peak are the most recognizable features of ECG signals. QRS-detection typically includes transforming each QRS complex into a single peak. The transformed peaks are then marked as QRS complexes or discarded based on threshold values, such as peak amplitude. Other possible thresholds include wave duration and peak interval length. Adaptive threshold values are preferred over fixed thresholds due to the variable nature of ECG signals (Sörnmo and Laguna, 2005). The QRS detector must be able to detect the QRS complex under various conditions, such as if the signal amplitude changes rapidly or the wave appears earlier than the average peak interval would indicate, as in the case of premature ectopic beats.

After the QRS complex has been detected, it is possible to look for other signal features around the QRS complex. However, the smaller waves are more demanding to detect especially from a noisy record. Detecting the P wave is more challenging than detecting the T wave, which always follows the QRS complex (Sörnmo and Laguna, 2005). The QRS-detection step is especially important because the rest of the analysis steps depend on it.

Wave delineation means detecting the outline of the ECG waveform, which includes finding the beginning and the end of the waves in the ECG. Duration and amplitude of the waves can be determined after the boundaries have been established. Wave delineation methods must also be able to detect a missing wave. Wave delineation can include special preprocessing in order to achieve optimal performance. For example, the P and T waves, and the QRS complex have different frequency components so it is natural to apply filters with different pass bands in order to detect them.

Amplitude thresholds could be used in defining wave and complex boundaries similar to QRS complex detection, however this method is sensitive to noise. Instead of thresholds, many wave delineation methods look for the slopes of the wave boundaries. The slopes are defined using the first derivatives of the signal. Signal derivatives/slopes can be compared to a reference value, a percentage of the maximum slope or a waveform template (Sörnmo and Laguna, 2005).

The initial steps of digital ECG processing included removing the noise and determining the QRS complexes, and possibly also the rest of the waves in the ECG. Further ECG signal processing steps can include feature extraction, selection, and classification. Machine learning methods are also applied in advanced ECG analysis. However, they are out of the scope of this thesis, and the reader can refer to the book by Murphy (2012) for more details.

Feature extraction means that specific details, such as peak amplitudes, are extracted from the ECG signal. There is a multitude of ECG signal features that can be used for classifying the heart beats and diagnosing arrhythmias. Computational methods, such as machine learning methods, can make use of all the features in Table 2 in addition to statistical features, and features produced by different transformation methods (Mar et al., 2011).

However, all the features that are created in the feature extraction step might not

be used in the classification step. *Feature selection* is used to choose only the relevant features, that is, those features that are the most successful in discriminating normal and arrhythmic beat types. Additionally, the extracted features might be further processed before the classification. Dimensionality reduction methods are a common approach to reducing and modifying the features before classification (Martis et al., 2013).

Finally, feature selection is followed by the *beat classification* step. Features of the ECG waves might be clustered and used for grouping the waves into different types, such as normal and ectopic beats. The chosen features can be compared to either predefined or dynamically created values or templates. The amount of different classification methods that are used in computational ECG analysis is enormous. For example, linear discriminants, the k-nearest neighbor method, and artificial neural networks have been widely used (Mar et al., 2011). Discrete wavelet transform has been used with dimensionality reduction methods to provide features for different classification methods, including neural networks and support vector machines (Martis et al., 2013). Neural networks are used to classify features created by various methods, such as higher order statistics, higher order spectra, and higher order cumulants. A comprehensive report of machine learning techniques used in ECG classification is given in the article by Jambukia et al. (2015).

Information gained in the advanced analysis steps is used to produce an automatic diagnosis. This computerized diagnosis can serve as a basis for the cardiologist who will go through the ECG record. In an optimal situation the cardiologist will then have to check only those parts of the lengthy ECG record that the analysis system has noted to differ from normal.

2.4.3 Methods of computerized ECG analysis

There is a multitude of ECG signal processing implementations developed over the years. Many implementations are based on similar methods, some of which are discussed in the following sections. The same methods can be used for different tasks, such as wave detection or classification. For a more comprehensive review of current methods one can see the article by Martis et al. (2014). The most important methods for this thesis are introduced next.

Derivative based algorithms make use of the characteristic slope of the QRS complex for QRS–detection or wave delineation (Kohler et al., 2002). The Pan-Tompkins algorithm is a well-known implementation for real-time QRS-detection, which utilizes the slope, amplitude, and width information of the waves to note them as QRS complexes or disregard them as artifacts or T waves (Pan and Tompkins, 1985).

Wavelet based QRS-detection and classification utilize the wavelet transform. Wavelet transform is localized in both time and frequency, unlike the Fourier transform, which only reveals the frequencies (Bentley and McDonnell, 1994). Therefore, it is possible to characterize the local regularities of signals, such as the ECG signal, by decomposing the signal using the wavelet transform (Mallat and Hwang, 1992). Wavelet based methods have also been used for signal preprocessing, arrhythmia

detection, heart rate variability (HRV) analysis, and signal compression (Addison, 2005). The strength of the wavelet method is better noise resistance compared to conventional methods and lesser computational complexity compared to, for example, hidden Markov models (HMM) (Li et al., 1995).

Adaptive filters that are used to manage fluctuating noise in ECG recordings are commonly based on the least mean square (LMS) or recursive least squares (RLS) algorithm (Singh and Yadav, 2010) (Milanesi et al., 2006). Adaptive filters have adjustable parameters, which are automatically adapted by the filtering system. However, there are also parameters that must be set before applying an adaptive filter. For example, the coefficient number in LMS filtering, which can be selected to maximize the output SNR or to optimize the relation between SNR, and unit process time (Yoon et al., 2008). Additionally, the number of iterations needed for convergence should be considered (Liu, 2011). Adaptive filters can also be combined with non-adaptive filters for optimal performance (Gholam-Hosseini et al., 1998). Example of a typical adaptive filtering system used in ECG noise cancellation is given in Figure 12.

Dimensionality reduction methods include principal component analysis (PCA), linear discriminant analysis (LDA), and independent component analysis (ICA). PCA reduces the data by projecting the data into components that maximize the variability. PCA has been applied together with other methods for arrhythmia detection and classification (Martis et al., 2014). LDA maximizes the discrimination among classes and has been used for ECG classification. ICA is also used to transform the multidimensional data into new components similarly to PCA and LDA, but instead of maximizing the variability it is based on maximizing the independence of the components. ICA has been used in, for example, feature extraction together with wavelet feature extraction in an arrhythmia detection system (Jiang et al., 2006).

There are also multiple other methods that are applied in ECG signal processing and analysis. However, describing them all in detail is out of the scope of this thesis. For example, genetic algorithms are used to optimize different parameters, such as filter parameters (Poli et al., 1995) or wavelet denoising parameters (El-Dahshan, 2011). Filter banks are used to separate signals into several frequency bands, which can be used as features for classification (Wieben et al., 1999). Filter banks are also applied in noise reduction (Łęski and Henzel, 2005) and beat detection (Afonso et al., 1999). Artificial neural networks are used to classify arrhytmias based on several features (Prasad and Sahambi, 2003). There are also many types of neural networks that have been used in beat classification (Ceylan et al., 2009). HMMs can be applied in various tasks in ECG analysis, such as, beat detection, delineation, and classification (De Lannoy et al., 2009; Andreao et al., 2006).

2.5 ECG artifacts and noise

Noise and artifacts are present in all biomedical signal recordings (Rangayyan, 2002). Strong noise or artifacts can make the signal virtually unreadable, hide small amplitude variations in the ECG, or even lead to wrong diagnoses. Consequently, it is important to separate disturbances from the signals in order to apply the signal

recording in diagnosis and monitoring.

2.5.1 Origin of ECG artifacts and noise

The ECG measurement setup determines the most important artifacts, and different methods must be applied for their removal. For example, patient monitoring systems are used commonly in hospitals. If the monitor is used in a surgery, the ECG recording is more likely to be affected by the electrical interference of the electrosurgical unit than by movement artifacts (Takla et al., 2006). On the contrary, a stress ECG is most likely disturbed by movement artifacts that originate from respiration, electrode movement, and skin resistance changes (Rangayyan, 2002, p. 265).

To be able to separate the signal of the heart from the noise, one should not only understand how the depolarization waves in the heart are transformed to the voltage signal in the ECG, but also the origin of the noise. There are multiple possible factors that can disturb the ECG signal, including electrical interference and motion (Neuman, 2009a). Artifacts from different sources have different typical characteristics, such as frequency spectrum and amplitude. Knowledge of the artifact's source and typical characteristics can help to separate it from the heart's signal.

Some of the most important noise and artifact sources are discussed in the following sections, in addition to some methods to prevent or reduce their influence on the ECG.

2.5.1.1 Electromagnetic interference

Electrical interference in ECG has been widely discussed in the book by Neuman (2009a), which was used as the main reference for the following section. Possible sources of electromagnetic interference include:

- Electrical signal related to muscles
- Cardiac defibrillation
- Electrical devices
- Powerlines

Electric interference can be caused by other signals coming from the patient's body (Neuman, 2009a). Not only the contractions of the heart muscles depend on electrical activity, but also the contractions of skeletal muscles. The electrical signal that creates skeletal muscle contractions is called the electromyogram. Electromyographic interference is more demanding to remove than, for example, powerline interference since its frequency content overlaps with the P-QRS-T complex. (Sörnmo and Laguna, 2005)

Cardiac defibrillation can cause large transients to appear on the ECG (Neuman, 2009a). The transient voltage can be much higher than the normal ECG waves recorded. Large electric pulses can cause the ECG amplifier to saturate and the gradual recovery from saturation will cause the ECG signal to stay disturbed for a while. Other sources of similar disturbances are severe motion of electrodes and static electricity shocks. The ECG can be protected from these high voltage input signals

using protection circuitry. Static electricity is reduced by using special materials in clothing and shoes.

Electromagnetic interference can also be caused by electrical devices, such as mobile phones and hospital equipment (Neuman, 2009a). However, quality instrumentation with high common mode rejection rate amplifiers are able to reject external electromagnetic interference. The driven right leg circuit is also used to reduce the common mode voltage.

Powerline interference at 50 or 60 Hz is usually caused by electric-field coupling between the powerlines and the ECG, or the powerlines and the patient, and can be minimized by shielding the ECG leads and grounding the shielding (Neuman, 2009a). However, if powerline interference is present in ECG regardless of the precautions it can be removed by, for example, bandstop filtering (Sörnmo and Laguna, 2005). The power lines can interfere with the ECG also by magnetic induction, as the magnetic field created by the power lines is picked up by the lead wires in the ECG. Magnetic field pickup can be minimized by reducing the loop created by the long lead wires. This is achieved by twisting the lead wires and keeping them close to the measurement subject.

2.5.1.2 The skin-electrode interface as an artifact source

Movement induces movement artifacts in the ECG by various methods. If the electrode moves with respect to the skin, it can cause a disturbance in the charge distribution in the skin-electrode interface (Neuman, 2009b). Movement artifacts are also induced by deformation of the skin (Tam and Webster, 1977), which can be caused by stretching or pressing the skin. When one electrode moves with respect to the skin and generates a temporary change in the potential distribution, a potential difference between the two electrodes in a lead will be recorded. For example, stretching of the skin changes the skin's potential by 5 to 10 millivolts (Neuman, 2009b). See Section 2.3.2 for details about the skin-electrode interface.

The non-polarizable Ag/AgCl electrodes are less susceptible to movement artifacts than polarizable metal plate electrodes. The electrode-electrolyte interface is more stable due to more constant concentration of ions at the interface in non-polarizable electrodes. However, the skin-electrode interface is still vulnerable to movement artifacts. Removing the stratum corneum and excess body hair will provide more uniform contact together with the electrolyte gel between the electrode and the skin (Crawford and Doherty, 2011, pp. 33–36). Light abrasion has been found to reduce both the skin potential and the change in skin potential when inducing a movement artifact by pressing the electrode (Tam and Webster, 1977).

Electrode motion can cause baseline wander, which is low frequency noise under 1 Hertz. Baseline wander can be caused by changes in the skin-electrode interface impedance, sweating, breathing, and other movements. Key methods in removing baseline wander include linear filtering and polynomial fitting (Sörnmo and Laguna, 2005). Highpass filtering that does not distort the signal is required to remove the baseline wander, so the cutoff frequency and phase response should be carefully designed (Gacek, 2011). However, the artifacts inflicted by motion will likely not be restricted to baseline wander. If the patient is moving a lot, as in a stress test ECG,

the movement related artifacts can reach several Hertz and higher amplitudes, and require more advanced filtering. Removal of these movement artifacts is discussed in the following sections. Comparison of baseline wander, movement artifacts, and muscle noise is provided in Figure 11.

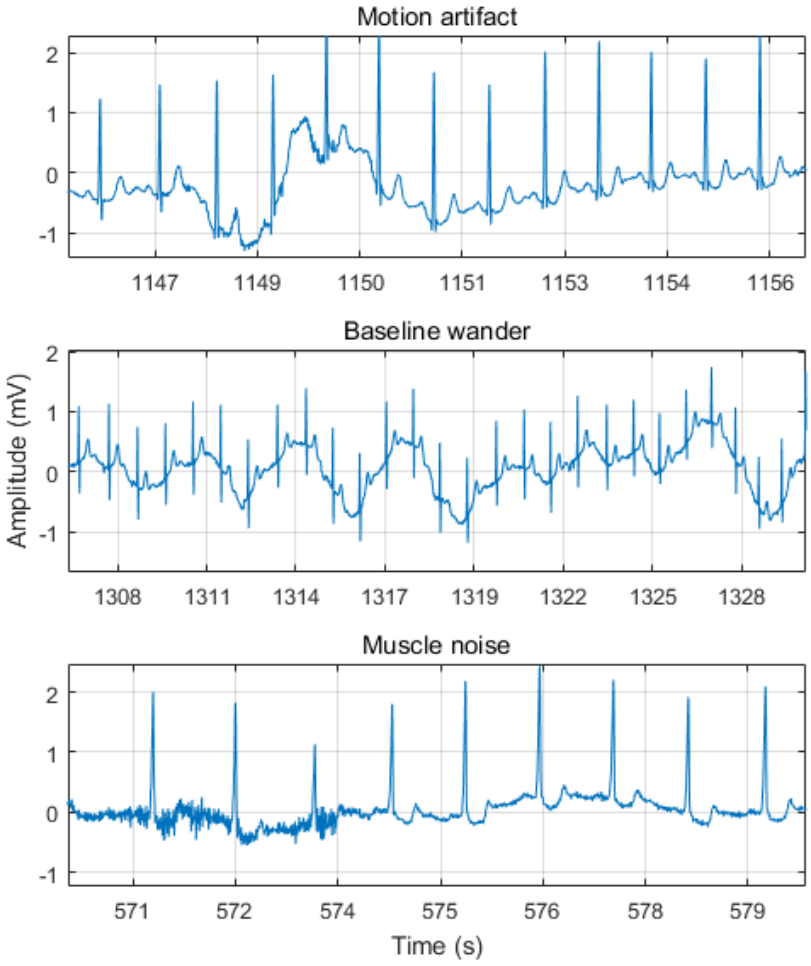

Figure 11: Types of disturbance that are related to movement on ECG signal. Movement artifact (top) on MITDB record 103, baseline wander (middle) on MITDB record 103, and muscle noise (bottom) on MITDB record 114.

It is not possible to avoid all motion during ECG recording, especially since physical activity is essential in some types of ECG. However, other non-computational measures can be used to reduce the effect of movement artifacts during stress ECG or ambulatory ECG. As discussed previously, the main source of movement artifacts when Ag/AgCl electrodes are used is the skin-electrode interface (Webster, 1984). Therefore, the instrumentation development should focus on making the skin-electrode interface more stable. For example, microneedle electrodes that are able to bypass the stratum corneum have been developed as an alternative to the Ag/AgCl electrodes, providing a more stable and conductive interface between the skin and the electrode (Forvi et al., 2012). It is also possible to reduce movement artifacts by simply

covering the electrodes and taping the ECG cables, but more efficient methods are also required (Lönnblad et al., 2005).

There are also simple measures that can be taken to improve computational ECG diagnosis. Minimizing the contribution of common technical difficulties can be achieved by performing a daily electrode change. The contribution of electrode condition and skin preparation is noteworthy; daily electrode change resulted in a 46% reduction in alarms by monitoring systems in a study by Cvach (2012).

2.5.2 Spectral contents of ECG and movement artifacts

The spectral contents of ECG signals vary with time, physical activity, and interestingly also due to heart related conditions such as myocardial infarction (MI) (Bhargava and Goldberger, 1981), in other words, a heart attack. This makes bandlimiting the ECG to remove noise quite complex. It is especially demanding to remove movement artifacts that overlap with the signal of the heart. Some important concepts regarding the frequency contents of ECG and movement artifacts are discussed next.

It is important to know which frequencies contain necessary information in the ECG for several reasons; to avoid filtering out crucial components, to isolate noise from artifacts, to separate the P-QRS-T waves from each other, and to identify possible changes or abnormalities in the P-QRS-T waves for diagnostic purposes. Both Fourier and wavelet transform based methods have been used to study the frequency spectrum changes related to cardiovascular diseases (Tsutsumi et al., 2014).

The spectral composition can be described by the power spectral density (PSD). It tells how much power each frequency has in a signal. The most important components lie within 1 to 10 Hz, including the QRS-complex, P, and T waves (Clifford, 2006). However, important components of the ECG signal would be missed if the signal was lowpass filtered as low as 10 Hz. A basic ECG recording might be bandlimited to 0.5 Hz - 40 Hz but even this limitation is too narrow to capture all diagnostically relevant information. The general recommendation is a frequency range from 0.05 to 150 Hz for diagnostic purposes, even though it will not eliminate baseline wander (Bailey et al., 1990). Yet wider frequency ranges can be needed for special purposes. For example, an increase in high frequency QRS components (150 - 250 Hz) have been found in patients with ischemic cardiomyopathy (Tsutsumi et al., 2014).

However, it is not possible to conduct detailed high frequency analysis if the recording contains noise. Even small amounts of movement related disturbances must be eliminated. Basic filtering methods are not well applicable as the frequency bands of the diagnostic components and the movement artifacts overlap (Afonso, 1993). For this reason multiple simultaneous recordings should be averaged and the patient must be very still for diagnosis based on spectral analysis (Tsutsumi et al., 2014). The frequency components are similar in different ECG leads, even though their energy differs (Clifford, 2006). This information can be utilized to recognize noise from the recording if multiple leads are available and the noise is not present in all of them.

2.5.3 Movement artifact related problems in ECG

In general, noise and artifacts make the ECG signal more difficult for the physician to read and interpret. For example, strong disturbance in the skin-electrode interface such as performing cardiopulmonary resuscitation (CPR) will obscure the ECG (Ruiz de Gauna et al., 2014; Fitzgibbon et al., 2002). However, stopping the CPR to enable rhythm analysis by automated external defibrillators (AEDs) has a strong negative effect on the probability of the patient's survival (Zhang et al., 2016).

Artifacts can have an effect on the ECG diagnosis made by computational methods even if the rhythm is detectable. Artifacts can affect the parameters that are derived from the ECG signal such as the heart rate, ST segment analysis, and arrhythmia detection (Takla et al., 2006). Especially movement artifacts cause false alarms in ECG monitoring systems, which hinders the clinicians' trust in the ECG monitoring (Lönnblad et al., 2005). Alarm fatigue has been declared as a common problem that might contribute to negligence and patient's death in the most severe case (Cvach, 2012).

2.6 Computational methods to manage movement artifacts

Methods to reduce movement artifacts have been studied for a long time and there are several approaches that can be jointly utilized (Webster, 1984). The following subsections will provide a more detailed overview of chosen computational methods. These methods can be roughly separated based on their goals. The two main goals are to detect or to correct signal quality. In some cases it is sufficient to determine if the ECG signal is acceptable or too contaminated by artifacts. More complex methods are required to actually remove the movement artifacts from the ECG without disturbing the ECG signal.

2.6.1 Methods to detect signal quality

ECG signal quality can be used to suppress false alarms in monitoring systems or for lead selection in multi-channel ECG. Signal quality indices (SQIs) can be used to estimate the quality of various biosignal measurements, including ECG (Mäntykangas, 2016). The SQIs can be based on different aspects of the signal, such as signal kurtosis, skewness, and QRS complex power (Behar et al., 2013).

Behar et al. (2013) constructed a method to evaluate ECG signal quality based on a machine learning approach. However, they noted that the same SQI should not be used to evaluate the quality of ECG signals in all cases. Some arrhythmias resemble noise according to certain SQI measures, and so different SQIs should be used with different rhythms. However, the development of a system that is able to choose the optimal SQI using machine learning techniques would require large amounts of annotated data (Behar et al., 2013). The benefit of determining the rhythm before selecting the SQI has been discussed in other studies as well (Li et al., 2014).

False alarm gating is one of the most interesting applications for SQIs. Abdelazez et al. (2017) developed a method to gate false ST segment deviation alarms in

ambulatory ECG based on a SQI. The index was based on measuring R-peak deviations from the ensemble average within 30 s windows. The false positives in the MI monitoring system caused by poor quality ECG were greatly reduced using the gating method. SQIs can be applied to other applications as well as false alarm gating. For example, Wang (2002) formulated a SQI to be used for automated ECG lead selection that is to find the lead that has the best quality. The SQI was based on the differences of QRS complex areas of successive complexes.

There are other methods in addition to SQIs that are used to assess signal quality. Redmond et al. (2012) developed a method to estimate signal quality from single channel ECG using a Parzen window classifier. The purpose of the study was to classify whether a reliable HR can be extracted from an ECG signal. Estimation of the reliability of HR or another signal feature is especially important in telehealth since ECG recordings that are operated by the measurement subjects themselves without supervision are especially prone to noise and artifacts.

Information from additional sensors or variables, such as lead impedance, can be utilized to estimate signal quality as well. Additional information can be used to monitor signal quality and gate false alarms similarly to the SQIs based on the ECG signal itself. Wiese et al. (2005) studied the applicability of lead impedance as an indicator of ECG signal quality, but found that there was no clear connection between DC impedance rise and movement artifact susceptibility. In addition to impedance, for example, acceleration has been estimated to give information about signal quality. Kishimoto et al. (2007) used 3-axis acceleration information from an accelerometer placed on the chest during sleep to classify noise as movement related. Body position changes were found based on the first derivative of the accelerometer signal.

2.6.2 Methods to separate movement artifacts from ECG

The basic methods for noise and artifact removal were introduced in Section 2.4, and more specific methods are discussed in the following sections. The implementations discussed next can be divided into two; methods that utilize only the ECG signal, and methods that utilize also additional variables. Methods that use only the ECG signal to reduce movement artifacts include, for example, time averaging, filter banks, wavelet transform (Mithun et al., 2011), and blind source separation (Romero et al., 2011).

Multiple implementations that utilize wavelets have been developed for movement artifact removal. Strasser et al. (2012) developed a method that estimates the artifacts using stationary wavelet transform and multiresolution thresholding for ECG signal preprocessing. However, many of the DSP methods distort the signal in addition to removing artifacts. Mithun et al. (2011) adjusted the level of wavelet based movement artifact removal so that the level of filtering would not distort the ECG signal.

Artifact removal can also be designed for a specific purpose to remove the effect of a well-known artifact source, such as CPR related noise. Zhang et al. (2016) developed a method to separate chest compression artifacts from ECG based on

an enhanced LMS method. The method was successful in separating ventricular fibrillation and sinus rhythm from ECG with different SNR levels. However, the artifact removal methods that are able to suppress movement artifacts can also affect the original ECG signal. That can lead to, for example, false positive irregular rhythm detections (Werther et al., 2009).

Blind source separation methods that apply PCA or ICA have been applied to separate ECG and noise in various studies (Romero et al., 2011). Blind source separation methods typically exploit multi-channel recordings, which reduces their applicability. Palaniappan and Khoon (2004) developed a single-channel PCA method to reduce noise from ECG, however the method was not tested using ECG with movement-artifacts. Furthermore, single arrhythmic peaks such as PVCs cause trouble to PCA based methods even though they are able to reduce noise (Palaniappan and Khoon, 2004).

Information about the body movements of the measurement subject can be used to identify movement-related noise in the ECG signal. Body movements might be detected directly from the ECG, even though activity identification is typically accomplished using inertial sensors (Preece et al., 2009). Pawar et al. (2007) utilized a recursively updated PCA based technique to detect body movement transitions, such as standing still to walking, in wearable ECG recordings. They did not use additional sensors to detect the movements. The study was conducted using a single lead electrode with lead II configuration.

2.6.3 Additional sensors to measure movement artifacts

Movement artifact removal can be based on recording another variable in addition to ECG. The additional variables can be related to movement or directly to skin stretch. They are recorded using supplementary sensor systems, which measure one or several variables, such as acceleration or impedance. However, using methods that utilize additional sensors and methods that are only based on the ECG signal itself are not necessarily mutually exclusive. Romero et al. (2011) suggested that the combination of both types of noise removal methods such as ICA and adaptive filtering could be beneficial. Several adaptive filtering implementations to reduce movement artifacts have been developed over the years, such as the ones that are discussed below. The general structure of adaptive filtering methods used in ECG noise or artifact removal can be seen in Figure 12.

Accelerometers are used to measure changes in velocity and are applied as the movement reference in many studies. Raya and Sison (2002) took advantage of accelerometer recordings in an adaptive filtering system to minimize artifacts in ECG measurements during cycling in a bicycle ergometer. The accelerometer was placed on the lower back, where the accelerations caused by walking or running can be detected. They studied the effect of using either one or two movement sensors as noise references and found out that the 2-axis reference distorted the ECG signal. Using the vertical axis as a noise reference was found to be especially successful, as the kinematic acceleration component in movement is focused on the vertical direction. The RLS algorithm was found superior to the LMS implementation in

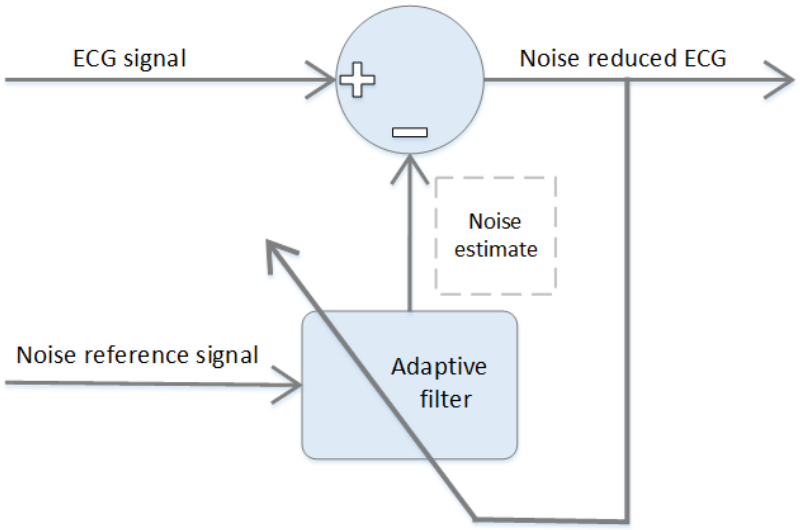

Figure 12: General structure of adaptive filtering in ECG noise or artifact reduction includes only a few components, as presented by Rangayyan (2002, p. 265).

improving the SNR with the cost of increased computational time.

However, placing the movement reference to one point would not necessarily capture all types of movement that cause skin stretch in vicinity of the electrodes. Early methods of movement artifact adaptive filtering were generally unsuccessful in achieving a good correlation between the additional variables and the artifacts because the methods that focus solely on capturing movement do not effectively capture the artifacts caused by skin stretch (Liu and Pecht, 2006).

Liu (2011) highlighted the need to place the additional sensor very close to the ECG electrode in order to catch artifacts caused by changes in the skin-electrode interface. A 3-axis accelerometer was placed next to the ECG electrode as the noise reference for adjusting the LMS algorithm. It was also noted that the nonlinear phase filter distorts the P and T waves, which could be harmful in applications that utilize other information besides the RR interval.

Tong et al. (2002) focused on the movement of the electrodes and compared the use of a 2-axis anisotropic magnetoresistive sensor to a 3-axis accelerometer in an LMS adaptive filter to reduce movement artifacts. The movement artifacts were inflicted by pushing the electrode or the skin, and pulling the lead wire. Better results were gained using the accelerometer data as the input to the adaptive filter, however low-level noise remained in the filter output.

Movement artifact removal is especially important in wearable ECG systems since they are more prone to artifacts than Ag/AgCl wet electrodes. Yoon et al. (2008) developed movement artifact reduction in a wearable ECG system. They used a 3-axis accelerometer as the noise reference for LMS filtering. Another implementation of movement artifact removal in wearable ECG system was developed by Jung and Jeong (2012). Instead of the commonly applied LMS method they applied empirical mode decomposition (EMD) in movement artifact removal. Acceleration data was used to adapt the filter level of the adaptive filter implementation. The filtering

technique was found to improve R-peak detection when the measurement subject was moving actively.

Methods that focus on capturing the skin stretch or the state of the skin-electrode interface have also been studied. Adding pressure on top of the electrode causes skin-electrode impedance variation and movement artifacts. Therefore, for example, pressure and impedance measurements can be used in adaptive filtering.

Liu and Pecht (2006) developed a system that captures the skin stretch via an optical sensor combined with a light emitting diode (LED) to capture the relative movement between the skin and the electrode. They were also able to determine the time lag between skin stretch and artifact in the ECG signal to be 0.28 seconds.

Pengjun et al. (2011) studied the applicability of movement artifact removal by adaptive filtering in a wearable electrode system. They integrated an optical displacement sensor and a thin film pressure sensor into the electrode in order to measure skin-electrode displacement and skin-electrode pressure. The skin-electrode pressure was found closely related to the movement artifacts in their system. Pressure or force has been applied also as the noise reference in adaptive CPR artifact removal by Berger et al. (2007). They applied adaptive filtering using compression force as the noise reference, however their testing was very limited.

In order to compare the use of different artifact references in adaptive movement artifact filtering, the references should be captured in the same system. Also different adaptive filters should be compared using the same data. Romero et al. (2012) compared the use of 3-axis accelerometers and skin-electrode impedance as the artifact reference input to RMS and different LMS algorithms. The combination of impedance and LMS sign-error algorithm was found best, however the filtering was found to distort the ECG. Another comparison was carried out by Hamilton et al. (2000). An LMS adaptive filter was implemented based on skin-electrode impedance and compared to filtering based on electrode bend sensor. Impedance and bend were found equally successful in artifact reduction but the impedance based method was concluded more practical. Electrode-tissue impedance based LMS adaptive filtering was also applied in the multisensor biomedical IC (MUSEIC) (Van Helleputte et al., 2015).

There are also alternative methods to exploit the artifact reference data to the LMS adaptive filtering, which is the most common approach. Kirst et al. (2011) applied wavelet transform to selectively remove artifacts based on skin-electrode impedance. The method was able to reduce false detections by 35% in dry-electrode ECG measurements. The purpose of selective filtering was to keep the ECG signal as non-disturbed as possible. Filtering typically inflicts slight changes in the ECG morphology in addition to artifact removal, so it is beneficial to only modify those parts of the signal that have severe artifacts.

Methods that focus on local movement might not catch artifacts caused by more general movements. For example, skin-electrode impedance has been found to correlate with local movement artifacts, such as pushing the electrode, but less with global artifacts, such as walking (Buxi et al., 2012). The ideal system to remove or identify movement artifacts would catch disturbances originating from different types of movement, and might combine several methods. Multiple sites and sensors should

be used in order to study the ideal combination of sensors for a system designed to reduce the effect of movement related artifacts in ECG.

There are various practical matters that should be considered when designing a sensor system to be used with ECG. Important factors to be considered include disturbance of the ECG measurement, flexibility and reliability of sensor attachment, comfort, and cost.

The weight of the sensor can affect the ECG measurement if the sensor is placed on top of the ECG electrode. Also, the heavier the sensor is, the more difficult it is to attach to the skin reliably. The tightness of the attachment combined with the weight of the sensor can also alter the vibration behavior of the skin (Forner-Cordero et al., 2008). Furthermore, the attachment should not disturb the movement of the measurement subject or cause pain. The cost of the sensors will also influence the applicability of the method and possibly limit the amount of sensors that can be used ata the same time.

Many of the systems designed for adaptive filtering of ECG use one of the two common methods to attach the sensors used to measure the additional variables. The first method is to integrate the sensor, such as an accelerometer, directly into the ECG recorder system (Jung and Jeong, 2012; Yang et al., 2008; Kim and Tewfik, 2015). This method does not allow flexibility for the sensor placement and does not allow the use of multiple sensors. Flexibility of sensor placement is essential if the effect of sensor location on the filtering result should be studied.

A more flexible method to attach the additional sensor(s) is to use a strap/belt (Kishimoto et al., 2007; Chung et al., 2008). Using a strap allows the sensor to be attached to a different location than the ECG measurement device. However, the strap should not interfere with the ECG measurement and so it can not be flexibly placed on the chest if multiple ECG electrodes are used. Using more than a few sensors attached to the body at the same time using separate straps is not applicable for practical reasons.

The accompanying sensors must be placed as close to the electrodes as possible in order to measure electrode movement or skin stretch at the electrode location, which is not possible using sensors attached to straps or integrated into the EGC recording device. There are various methods to secure the additional sensors directly to the ECG electrodes reported in the literature, including attachment to the electrode foam by metal barbs (Hamilton and Curley, 1997), connection to ECG lead wire caps (Tong et al., 2002), and sticking to ECG electrode by permanent adhesives and lamination (Pengjun et al., 2011). However, these methods do not allow easy removal, which is required for the use with common disposable silver/silver chloride ECG electrodes. Direct attachment to electrodes seems to be more common when wearable systems, such as fabric electrodes are used. Wearable electrodes are more prone to movement artifacts and the additional sensors can be, for example, sewed to the electrode location (Milanesi et al., 2006). However, the sensors should also be able to be attached to skin, which is not possible by the methods described above.

The attachment of sensors, such as accelerometers, directly to skin using adhesive tape has been widely reported in the literature (Kitazaki and Griffin, 1995; Koivisto et al., 2015; Pandia et al., 2010). Also complete devices that use adhesive tape-like

methods to attach ECG measurement systems and other sensors have been developed in the recent years (Kit et al., 2013; McGinnis et al., 2016).

Another factor that should be considered when designing the attachment of the additional sensors is the force provided by the attachment (Forner-Cordero et al., 2008). Vibration of the skin and soft tissues causes distortion during movement measurements by inertial sensors, such as accelerometers. The force provided by a bandage-like attachment modifies the system's stiffness. The lower the force the lower the natural frequency of the system is. However, according to the study by Forner-Cordero et al. (2008), the weight of the elastic bandage does not affect the system significantly. It could be hypothesized that the area and tightness of a tape-like attachment would affect the system similarly. However, if the tape does not go all the way around the limb or torso, the tightness is supposed to stay relatively low.

The noise reference should ideally correlate well with the artifacts but not with the ECG signal. Correlation with the ECG can be a problem with accelerometer recordings. If the sensor is placed close to the heart it could record the seismocardiogram, which is correlated with the ECG (Kirst et al., 2011). Accelerometers have been used to obtain heart sounds from the chest, which is an alternative heart rate measurement method.

3 Research material and methods

The research material, software that was used, and finally the methods that were implemented in the research are covered in this chapter.

3.1 Materials

Both open ECG databases and experimental recordings made in Aalto were utilized in this thesis. Details of the origin of the research materials, including measurement equipment and software, are provided in the following subsections.

3.1.1 Software and algorithms

MATLAB® R2017a (Version 9.2) by MathWorks, Inc. was used for signal processing, algorithm testing, and producing statistics and graphs. Several MATLAB® tools from PhysioNets software library called the PhysioToolkit were used in reading and processing ECG data. The WFDB Toolbox for MATLAB and Octave (Silva and Moody, 2014) was used to process the ECG records. Each software tool used is mentioned in the methods section.

Three open source algorithms were tested in MATLAB® in order to study the effect of noise on ECG signal quality and automated ECG analysis. Each method is briefly discussed in the following section. R-Peak or QRS complex detection was used as the analysis measure.

3.1.1.1 Algorithm 1

The first algorithm was used as an instance of the popular Pan-Tompkins algorithm, which was designed for real-time QRS-detection by Pan and Tompkins (1985). The implementation used in this thesis was written by Sedghamiz (2014), and is available in MATLAB Central File Exchange.

The original Pan-Tompkins algorithm was implemented in assembly language and was optimized for speed, however the algorithm used in this thesis was implemented in MATLAB®. The algorithm exploits only one channel because the algorithm was originally designed for Holter devices and Holter recordings have typically only one channel with acceptable SNR.

The algorithm follows the general structure visualized in Figure 10. The first step is a series of low and high pass filters that comprise a digital bandpass filter. After noise removal, the signal is differentiated in order to get information about the signal slope. The signal is further processed by squaring, which helps to separate the QRS complexes from T waves that could otherwise cause false positive QRS-complex detections. Squaring makes each data point in the ECG signal positive and accentuates high frequencies, which are typically caused by QRS complexes.

The slope information alone is not enough to separate all QRS complexes. Some QRS complexes are larger and longer than usual and have less steep slopes, that is, smaller derivatives (Arzeno et al., 2008). A moving window integrator is described in the original article to obtain additional waveform information (Pan and Tompkins,

1985). This step is realized as a moving average with a 150 ms window in the MATLAB® implementation (Sedghamiz, 2014). The window should capture most QRS complexes but not merge the following T waves with them (Pan and Tompkins, 1985). However, QRS complex durations over 150 ms can be found in, for example, heart failure patients (Kashani and Barold, 2005).

The output of the preprocessing stages is a filtered and averaged signal that highlights the supposed QRS complexes that are reduced into simple peaks. The decision stage is applied after the preprocessing and so adaptive rules are used to determine which peaks are finally marked as QRS complexes. Firstly, locations and amplitudes of the local maxima are found using the function findpeaks() in MATLAB® with the minimum peak distance set to 200 ms. The rest of the decision stage is based on determining whether the peaks are caused by QRS complexes, noise or T waves. The decision is based on adaptive thresholds for peak amplitude, noise amplitude, RR interval, and peak slope information. If a QRS complex is not found within a specified window based on the average RR length, the threshold is lowered and a search back is triggered. (Sedghamiz, 2014)

3.1.1.2 Algorithm 2

The second algorithm is the open source QRS-detection algorithm wqrs, which is available in the WFDB Toolbox (Silva and Moody, 2014). The algorithm is described in more detail in the article by Zong et al. (2003). The algorithm consists of preprocessing and decision stages similarly to Algorithm 1, but is less complex. Preprocessing includes only low-pass filtering and curve length transformation. Low-pass filtering is conducted to remove high frequency noise prior to curve length transformation. ECG curve length corresponding to the QRS complex is longer than the other parts within a suitable window. Therefore searching for a local maximum curve length will provide the QRS complex location. The window length used in Algorithm 2 is 130 ms (Zong et al., 2003).

The decision stage of Algorithm 2 consists of two parts, as describer by Zong et al. (2003). The purpose of the decision stage is to search for QRS complexes and find their outlines. Adaptive thresholding is used to search for the QRS complexes in the length transform. The threshold value is increased or decreased based on the the maximum length transform value of the detected QRS complex. After a length transform signal that surpasses the threshold has been found, the second step is searching for QRS complex onset and end locally. Finding the QRS complex onset location is based on searching for local minimum prior to the threshold crossing point. Finding the wave end is based on searching for local maximum after the crossing point. The minimum peak distance, namely eye-closing period, is set to 250 ms in Algorithm 3 (Zong et al., 2003).

3.1.1.3 Algorithm 3

The algorithm discussed next is based on the article by Pal and Mitra (2010). The implementation used in this thesis was developed by Selva (2011) and is available in MATLAB Central File Exchange. Only the R-peak detection parts of the implementation are applied in order to evaluate how the method is affected by increased noise

levels.

The steps necessary for locating the R-peaks are wavelet decomposition, coefficient selection, and finally R-peak detection (Pal and Mitra, 2010). The wavelet and the decomposition level used are chosen as described in the original article. Dauchebies wavelet 6 (db6) with level 8 as the highest decomposition level is applied in the implementation. Dauchebies wavelet 6 was chosen because of its resemblance of the QRS complex. Dauchebies wavelet 6 is visualized in Figure 13.

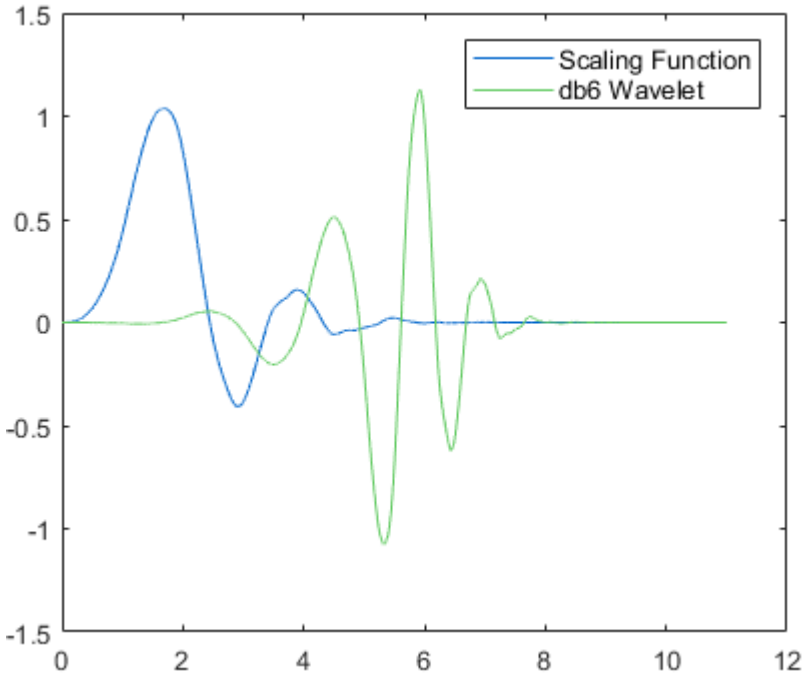

Figure 13: Dauchebies wavelet 6

MATLAB®'s Wavelet Toolbox (MathWorks, Inc., 2017a) is exploited in the MATLAB® implementation to create the wavelet decomposition and reconstruct the wavelet coefficients d1-d8. The QRS complex is best represented by the coefficients d3-d5 and so the signal can be reconstructed as a sum of the three coefficients (Pal and Mitra, 2010). R-peak detection is based on the signal e11, which is calculated according to the Equation (3). The R-peaks are located based on e11 amplitude and peak distances.

$$e1 = d3 + d4 + d5 \tag{2}$$

$$e11 = |e1 \cdot e1| = e1^2 \tag{3}$$

3.1.2 MIT-BIH Databases

The data used in noise testing is from the MIT-BIH Arrhythmia database (MITDB) (Moody and Mark, 2001), which is available in PhysioNet's PhysioBank (Goldberger

et al., 2000). PhysioNet includes access to large collections of physiological signal recordings and open source software to process the recordings.

The MIT-BIH Arrhythmia Database includes 48 half-hour signal fragments taken from 47 subjects. The recordings that are available in PhysioBank are fragments from different 24-hour ambulatory ECG recordings collected at Boston's Beth Israel Hospital. The 48 records were chosen from a set of 4000 records. The first 23 recordings were selected randomly and the last 25 were chosen so that important uncommon arrhythmias would also be present in the small sample set (Moody and Mark, 2001).

Each of the 48 records comprises three separate files; a signal file with the extension .dat, a header file with the extension .hea, and a file with the reference annotations with the extension .atr. The header file is written in ASCII text and includes information about the signal recording in the .dat file, such as the record name, number of channels, sampling frequency, and format of the signal (.dat) file. The records in MITDB have been digitized at 360 samples per second and include the signal from two channels. They are stored in format 212, which is a 12-bit binary format described by Moody (2015). The annotation file includes the annotation type codes and the annotation times in binary format that correspond to the annotations originally made by cardiologists on paper.

The MIT-BIH Arrhythmia database was chosen as the material for testing the effect of noise on ECG processing algorithms for several reasons. The data is publicly available, well described, and annotated. MITDB includes carefully inspected annotations made by cardiologists in addition to the signal records themselves. These annotations are used as a reference for the computationally made detections.

A noise recording from the MIT-BIH Noise Stress Test Database (NSTDB) was used to add noise to the records of MITDB (Moody et al., 1984). The noise file used was the record *em* from the database, which resembles real-life electrode movement artifacts.

3.1.3 Measurement equipment

Several sensors and other equipment were utilized in the experimental research that is discussed in this thesis. The experimental research was conducted by Aalto University staff, in the facilities of Aalto University department of Electrical Engineering and Automation.

ECG recordings were made using a Faros 360 wearable ECG recorder by Mega Electronics Ltd. 3-channel ECG was recorded using 1000 Hz sampling frequency and 3-channel acceleration was recorded using 100 Hz sampling frequency. The ECG setup, including electrode placement, is visualized in Figure 14. The three ECG channels correspond approximately to leads I, II and V_1, depending on electrode locations. The data from the ECG device was uploaded into a PC in European Data Format (EDF). EDF is a binary data format, which is similar to the MIT-dataformat, but it includes the header in the same file as the measurement output data. EDF was originally designed for storage of polygraphic recordings (Kemp et al., 1992).

Two different disposable Ag/AgCl electrodes were used in the ECG recordings

made with the Faros 360 device. The first ones were Ambu BlueSensor VLC ECG electrodes with 68 mm diameter, which were used in the illustrative case study. The second ones were Kendall ECG Electrodes (H135SG) with 35 mm diameter. Both electrodes have conductive gel and adhesives to enable contact to the skin.

Inertial mesurement units (IMUs) were used to measure movement during ECG recording. The IMUs used were MetaWearCPRO devices by MbientLab. Each sensor has a 3-axis accelerometer, 3-axis gyroscope, 3-axis magnetometer, and an additional barometer, temperature sensor, and light sensor. The accelerometer and gyroscope sampling frequencies are 100 Hz, and the magnetometer sampling frequency is 20 Hz. The IMU setup is visualized in Figure 14. The IMUs were attached to the ECG electrodes and skin using Micropore surgical tape with 12.5 mm width by the 3M company.

3.2 Methods

Three main methods were used in this thesis. A small illustrative study to test the ECG device during movement was followed by a simulation study, and finally a small laboratory experiment with IMUs and ECG recording was conducted. All of the methods are discussed in the following chapters with necessary detail.

3.2.1 Simulation to study the effect of movement

The effect of incrementally increasing the strength of movement artifacts was studied using a simulation. Parameters of the simulation were set so that the simulation would correspond to a situation where moderate movement is present during ECG recording.

3.2.1.1 Finding suitable parameters

A small experimental study was needed prior to the actual simulation study. This illustrative case study was conducted to visualize the effect of movement artifacts on ECG recordings. The Faros 360 ECG device was used to record ECG during different activities, such as sitting on a chair and waving hands. The recording made in this study was used as a reference for setting the noise level in the following computational study. The recording was also visually compared to the noise record used in the computational study to check that the artificial noise looks relatively similar to the real noise in the Faros 360 recording.

3.2.1.2 Quantifying the effect of movement artifacts on ECG algorithms

A simulation study using database ECG records was conducted to study the effect of movement artifacts on ECG algorithms. The performance of several algorithms was tested in varying conditions by adding movement artifact-like noise to the MIT-BIH Arrhythmia database. The function 'rdsamp' from the WFDB toolbox (Silva and Moody, 2014) was used to read the signal records and the noise record directly from PhysioBank into MATLAB®. In MATLAB®, the noise record was added to the ECG records to create artificially noisy records. A similar method has been described

in the MIT-BIH Noise Stress Test Database (Moody et al., 1984) and applied in previous studies (Mithun et al., 2011).

Noisiness of the records could be modified by using a coefficient by which the noise level is defined. Equation (5) is derived by simply adding the coefficient a to Equation (1). Separate coefficients were defined for each signal and each noise level according to Equation (6).

Different SNRs were tested, and the noise levels were set so that the signal quality of the treated MIT-BIH records was similar to the recordings made in the illustrative case study. The following equations describe the relation between the predefined $\mathrm{SNR_{dB}}$ values and the coefficient a:

$$\mathrm{SNR_{dB}} = 10 \log_{10} \left(\frac{P_{\mathrm{signal}}}{\mathrm{a}\, P_{\mathrm{noise}}} \right) \tag{4}$$

$$\Leftrightarrow \mathrm{a} = \frac{P_{\mathrm{signal}}}{P_{\mathrm{noise}}} \cdot 10^{-\mathrm{SNR_{dB}}/10} \tag{5}$$

$$= \frac{1/N \sum_{n=1}^{N} |\mathrm{signal}_n|^2}{1/N \sum_{n=1}^{N} |\mathrm{noise}_n|^2} \cdot 10^{-\mathrm{SNR_{dB}}/10} \tag{6}$$

$$= \frac{\mathrm{RMS_{signal}}^2}{\mathrm{RMS_{noise}}^2} \cdot 10^{-\mathrm{SNR_{dB}}/10}, \tag{7}$$

in which SNR_{dB} is the desired SNR level in decibels, P_{signal} is the signal power, P_{noise} is the noise power, $signal_{\mathrm{n}}$ is the signal voltage amplitude observation at point n, $noise_{\mathrm{n}}$ is the original noise voltage amplitude observation at point n, RMS_{signal} is the RMS value of the signal and RMS_{noise} is the original RMS value of the noise.

The function rms() in MATLAB® (MathWorks, Inc., 2017b) was used to calculate the root-mean-square (RMS) levels according to the Equation (7). SNR values were used to set the coefficients individually for each record, channel and noise level. Four signal types (three noise levels + the original signal) and 48 records total 192 test cases with two channels each. The noise signals are scaled by $\sqrt{\mathrm{a}}$, where a is the individual noise level coefficient calculated according to the Equation (7).

3.2.1.3 Statistics

Multiple algorithms were used to process both the original MIT-BIH records and the noise-contaminated MIT-BIH records. QRS complexes were detected from all 192 test cases with three methods, namely Algorithms 1–3. The algorithms were described in Section 3.1.1. The effect of noise on the performance of the algorithms was estimated by comparing several detection statistics. The statistics were produced using the bxb routine from the WFDB software package for MS-Windows (Silva and Moody, 2014). Bxb is a beat-by-beat annotation comparator that produces beat-by-beat performance statistics. It uses match windows to find matching annotations so the detections made by the algorithm do not have to have the exactly same timing as the reference annotations. The default match window is 0.15 seconds.

Sensitivity is one of the most important qualities of a QRS-detection algorithm. It is the probability that the algorithm is able to detect the QRS complex if there

is a QRS complex present at some point. QRS-detection sensitivity is calculated according to Equation (8). However, sensitivity alone is not enough to characterize the function of QRS-detection methods. Even if the algorithm had 100 % sensitivity, it might not be working well since sensitivity does not take false positive detections into account. For example, an algorithm that was only optimized for sensitivity could produce a lot of false R-peak detections. Therefore, another statistic called positive predictivity is commonly used to characterize QRS-detection algorithms in addition to sensitivity.

Positive predictivity, also called precision is the probability that the QRS-detection made by the algorithm was actually a QRS complex. The higher the precision, the less false QRS-detections the algorithm makes. QRS-detection positive predictivity is calculated according to Equation (9).

$$\text{Sensitivity} = \frac{\text{True Positives}}{\text{True Positives} + \text{False Negatives}} \cdot 100\%. \tag{8}$$

$$\text{Positive predictivity} = \frac{\text{True Positives}}{\text{True Positives} + \text{False Positives}} \cdot 100\%. \tag{9}$$

True positives are correctly detected QRS-complexes, false negatives are QRS complexes that were missed by the algorithm and false positives are false QRS-complex detections made by the algorithm.

More specific information about the false negative beats was created by a similar method to bxb. 150 ms maximum absolute difference in R-peak detection time was allowed. Peaks that were not found by the algorithms were classified according to beat type. The beat types used in this classification are based on the golden truth annotations similarly to bxb, but the classification that is reported contains more classes, whereas bxb sorts the beats into normal, PVC, fusion, and non-classifiable beats.

3.2.2 Combined ECG and IMU measurements

An experimental study was conducted to study movement reference combinations. The goal of this initial study was to evaluate the measurement setup and to estimate its capability to capture movement. Simultaneous ECG and movement recordings were conducted using several IMUs and ECG electrodes. ECG and movement recordings were collected from a healthy volunteer. In total four ECG recordings were made, during which the measurement subject performed different activities.

The measurement protocol was designed so that different activities that are expected to cause movement artifacts to the ECG signal would be represented. Each of the first three movements was performed twice. The first movement in the protocol is rolling from back to side. A similar movement appears while sleeping, and might cause severe artifacts to ECG. The second movement is pulling the ECG wire below the ECG recording device while standing, which can occur during many daily activities, such as when getting dressed. The third movement is horizontal shoulder rotation. More specifically, this movement is called 90° lateral rotation followed by medial rotation of the upper limb while the forearms are in 90° flexion. Similar

movements might occur while talking on the phone or getting dressed, for example. The fourth and the last movement in the protocol was walking a few steps up the stairs and then returning.

The Faros 360 device was connected using five electrodes. In addition, five inertial measurement units (IMUs) were attached above the electrodes using medical tape. Schematic of the measurement setup is given in Figure 14.

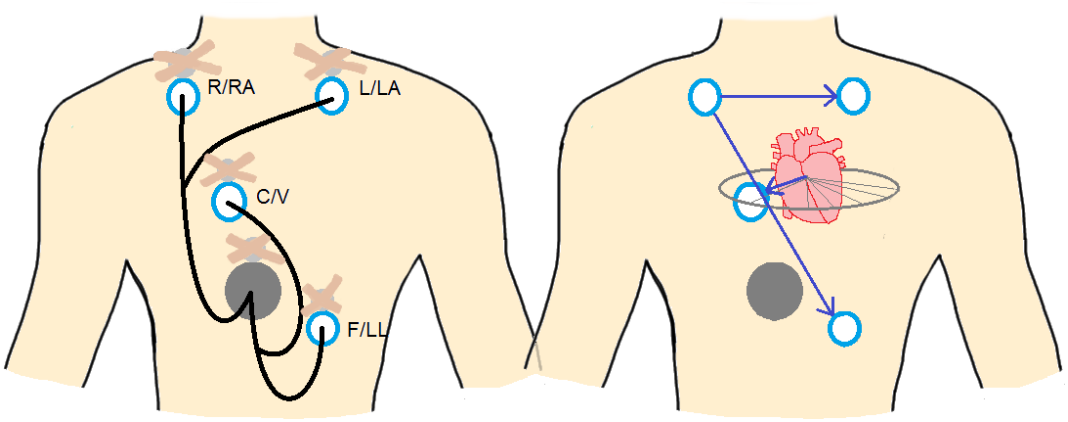

Figure 14: Schematic of the combined ECG and movement measurement setup. Connection of the electrodes and IMUs is visualized on the left and approximations of the lead directions that correspond to the ECG channels 1–3 are visualized on the right. Channel 1 is lead I (RA to LA), channel 2 is lead II (RA to LL), and channel 3 is lead V_1. The figures are not in scale, but only an approximate guide.

A separate ECG recording was made for each of the four movements in the protocol. The ECG device was switched on approximately 20 seconds before performing each movement to allow the baseline to settle. The IMUs were not switched off during the measurement, but data from each IMU was logged into a separate file. Data from the IMUs was transferred from the internal memory of the IMUs to a mobile device via Bluetooth and transferred to a PC. Also the data collected by the ECG recording device was transferred to a PC. Both signals were then read and analyzed using MATLAB®.

The measurements made by the Faros device and the five IMUs have to be synchronized since they do not have a common time axis and the measurements begun at slightly different times. A simple heel-drop movement was used as a mechanical reference signal in the beginning of the measurements. The movement should cause a clear peak in both the IMUs and the Faros device's accelerometers. The signals can then be synchronized by calculating the time-difference between the peak in IMUs and Faros. Simple mechanical synchronization was supposed to provide acceptable accuracy for short laboratory experiments.

Firstly, the effect of the movements 1–4 on ECG data quality on each ECG channel was evaluated visually. The severity of the movement artifacts was quantified as points from 1–4, from lowest to highest. Also the relationship between the artifacts and the different sensor signals from the IMUs was evaluated visually. Visual inspection is not only convenient, but also a good method to check the sanity of the results from

other approaches. The effect of movement is also studied by checking the results of automatic QRS-detection from the records by Pan-Tompkins algorithm. However, the records are so short that statistics are not produced as they would be based on such few samples.

Relation between the ECG and IMU data was also evaluated by calculating the Pearson correlation coefficients for each IMU channel-ECG channel combination. Sample Pearson correlation is given by the Equation (10).

$$\text{Correlation} = \frac{\sum_{i=1}^{n}(x_i - \bar{x})(y_i - \bar{y})}{\sqrt{\sum_{i=1}^{n}(x_i - \bar{x})^2}\sqrt{\sum_{i=1}^{n}(y_i - \bar{y})^2}}, \tag{10}$$

where n is the sample length, i is the sample number and $\bar{x}$ is the sample mean for signal x, $\bar{x} = \frac{1}{n}\sum_{i=1}^{n} x_i$ and $\bar{y}$ is the sample mean for signal y, $\bar{x} = \frac{1}{n}\sum_{i=1}^{n} y_i$.

4 Results

This chapter will cover all the results and aim at answering the research questions.

4.1 Simulation results

Results from the simulation study that used an artificial electrode movement artifact recording to create increasingly noisy record are given in this subsection. Prior to the simulation results, results from the illustrative case study are given.

4.1.1 Results from the illustrative case study

A realistic movement artifact level was defined according to the measurement setup described in the methods section. The noisiness of the ECG recording made by Faros 360 during different activities was compared to the MITDB record 100. Artificial noise was added to the MITDB record in different amounts. The noisiness of the records was found to look similar when the SNR of the MITDB was set between 5–9. Furthermore, the artificial movement artifacts in record em appeared similar enough to the noise in the real ECG recording. The noise levels were named as low, medium, and high, with the corresponding SNRs set as 9, 7, and 5. The chosen noise levels are visualized in Figure 15.

4.1.2 Algorithm performance statistics

QRS-detection sensitivity by signal noise level is visualized in Figure 16. Median sensitivities are represented by red horizontal lines and mean sensitivities are represented by orange dashed lines. QRS-detection positive predictivity by signal noise level is visualized in Figure 17. Median positive predictivity values are represented by red horizontal lines and mean positive predictivity values are represented by orange dashed lines. The influence of outliers on the detection statistics is significant, and so the median describes the effect better. The outliers could be caused by the noise that was already present in some original MITDB records.

The QRS-detection sensitivity of all three algorithms is affected by the increase in the artificial movement artifact level. However, the strength of the impact varies. The algorithms have different pre-processing stages to filter out noise and artifacts, which partly explains why they are affected differently.

The effect of increased noise level on QRS-detection positive predictivity is stronger than the effect on sensitivity. For example, the median sensitivity of Algorithm 2 drops only 0.32%, but median positive predictivity drops as much as 16.30%. According to the results, the amount of false positive peak detections rises substantially as the noise level is gradually increased for all algorithms.

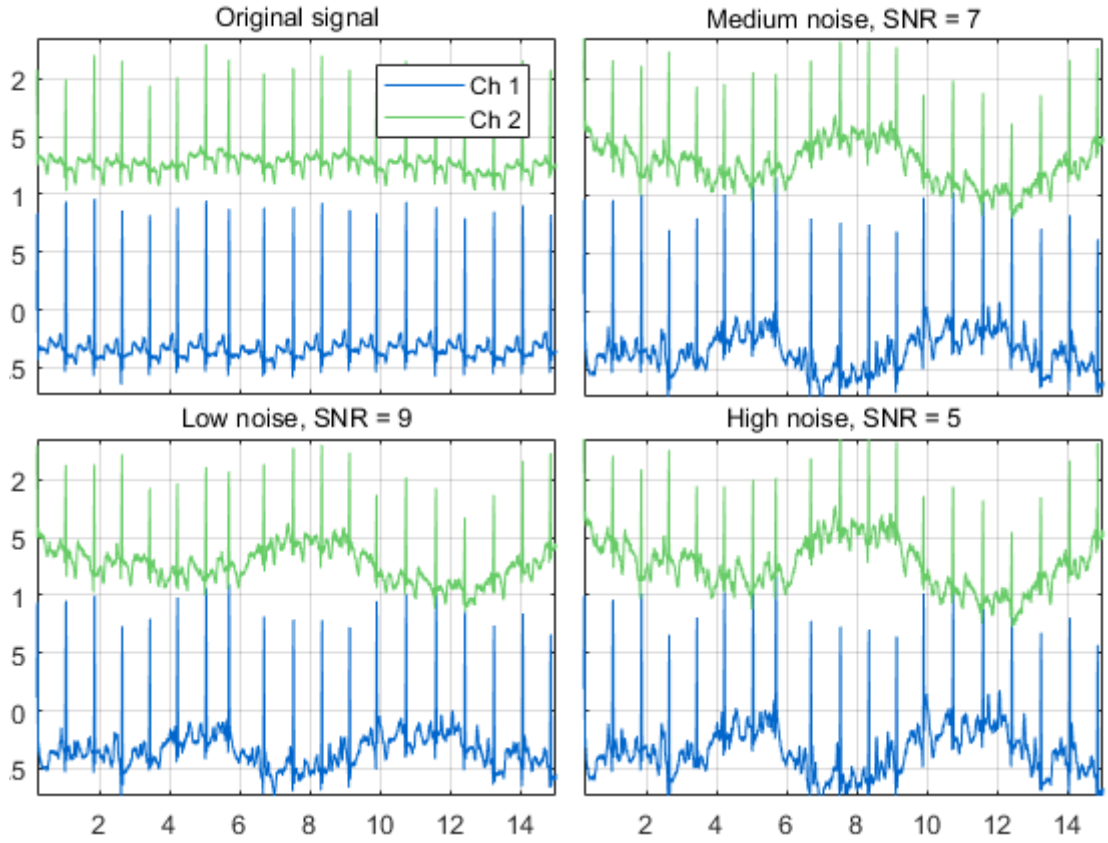

Figure 15: Noise was added in different levels to MITDB record 100. The noise record used to create the records mimics electrode movement artifacts.

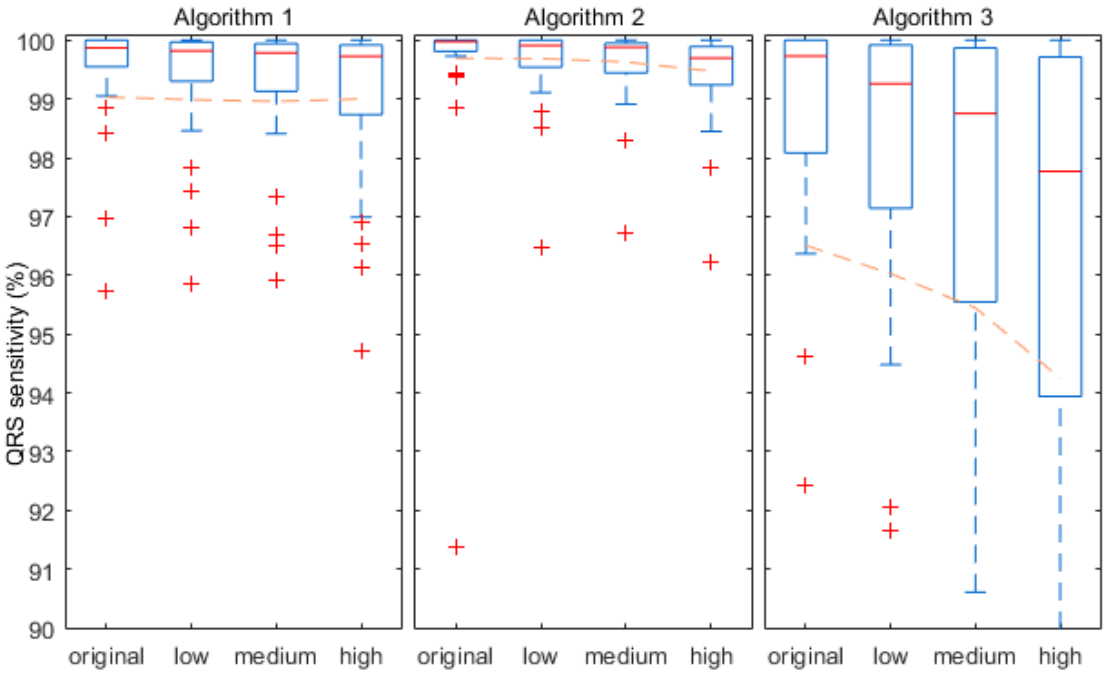

Figure 16: QRS complex detection sensitivity values are given by noise levels for Algorithms 1–3.

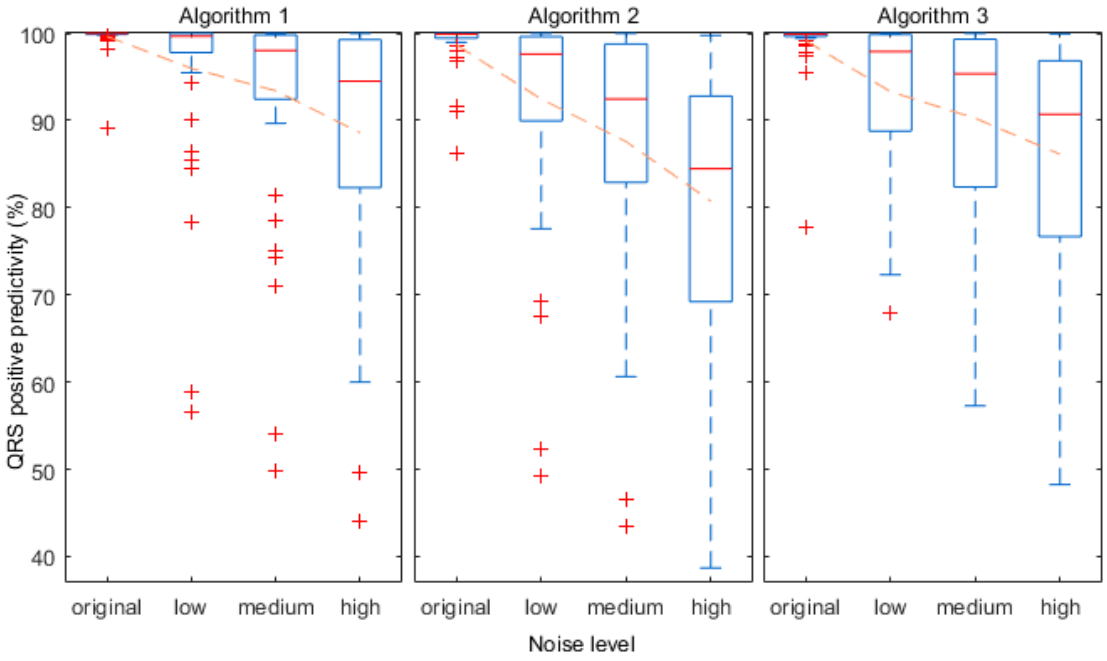

Figure 17: QRS complex detection positive predictivity values are given by noise levels for Algorithms 1–3.

Details about the types of beats that were missed by the algorithms are given in Table 3. In general, each beat type is more likely to be missed as the noise level increases as expected. However, the effect is less clear for Algorithms 1 and 2, which have the best sensitivity. Also, normal beats are more likely to be detected than other beat types, regardless of the noise. The type of the non-normal beat seems to have an effect on how likely it is detected as well. PVCs are the most likely beat type to be missed by the algorithms. As expected, the algorithms have different detection probabilities for the beat types since they use varied detection principles. For example, Algorithm 3 is clearly more likely to miss PVCs than the other algorithms.

More specific false negative classification is given in Table 4. The results for normal and PVCs are not completely identical to the results in Table 3, since the results in the first FN table were created by bxb and the results in the second FN table were calculated directly in MATLAB®. However, as can be seen the PVCs are most likely to be missed according to both tables. Furthermore, atrial premature beats are more easily detected than PVCs by all algorithms, and even better detected than normal beats by Algorithms 1 and 2. Detection of all beat types appear to get gradually worse due to rising the noise level. However, atrial premature beat detection by Algorithm 1 and LBBB detection by Algorithm 3 seem to get better with the rising noise level.

All in all, the results in Tables 3 and 4 suggest that even though different beat types have different correct detection probabilities, they are mostly affected similarly by noise.

Table 3: False negatives for each algorithm, noise level, and beat type. N = normal beat, V = PVC, F = Fusion of ventricular and normal beat, Q = Non-classifiable beat

Algorithm	Noise level	Beat type that was missed			
		N (pcs/%)	V (pcs/%)	F (pcs/%)	Q (pcs/%)
Algorithm 1	Original	644/0.83	146/2.39	7/1.12	16/0.24
	Low noise	612/0.79	177/2.90	9/1.44	69/1.02
	Medium noise	601/0.77	198/3.25	10/1.61	90/1.33
	High noise	525/0.68	208/3.49	9/1.44	145/2.14
Algorithm 2	Original	219/0.28	41/0.67	7/1.12	6/0.09
	Low noise	219/0.28	40/0.66	8/1.28	6/0.09
	Medium noise	271/0.35	38/0.62	7/1.12	7/0.10
	High noise	406/0.52	38/0.62	8/1.28	9/0.13
Algorithm 3	Original	2258/2.90	555/9.10	14/2.25	20/0.29
	Low noise	2514/3.23	671/11.00	17/2.73	91/1.35
	Medium noise	2901/3.73	735/12.05	18/2.89	168/2.48
	High noise	3707/4.77	874/14.33	22/3.53	285/4.20

Table 4: False negatives for each algorithm, noise level, and beat type. N = Normal beat, V = PVC, A = Atrial premature beat, R = Right bundle branch block beat, L = Left bundle branch block beat, P = Paced beat

Algorithm	Noise level	Beat type that was missed					
		N (%)	V (%)	A (%)	R (%)	L (%)	P (%)
Algorithm 1	Original	0.78	2.66	0.12	0.00	0.16	0.40
	Low noise	0.72	3.07	0.16	0.00	0.30	1.07
	Medium noise	0.71	3.32	0.12	0.01	0.33	1.34
	High noise	0.62	3.37	0.04	0.03	0.33	2.01
Algorithm 2	Original	0.30	0.70	0.04	0.01	0.05	0.04
	Low noise	0.30	0.70	0.04	0.08	0.05	0.03
	Medium noise	0.38	0.66	0.04	0.14	0.06	0.04
	High noise	0.52	0.66	0.16	0.26	0.28	0.06
Algorithm 3	Original	2.09	9.14	3.61	0.11	12.61	0.21
	Low noise	2.43	11.08	3.69	0.70	11.96	1.22
	Medium noise	2.87	12.06	3.93	1.85	11.78	2.40
	High noise	3.75	14.21	4.08	4.15	11.65	4.10

An example of a typical false positive beat detection is visualized in Figure 18. The movement artifact at approximately 516 s is falsely detected as a QRS complex by all the algorithms. The location of the movement artifact peak is similar to a PVC peak that is one of the most common abnormal peak. The image is an example of the situation where a movement artifact mimics an atypical heart beat. Parameters of the algorithms can not be set so that the artifact would be recognized as noise, because then the algorithms would be likely to miss actual PVCs as well.

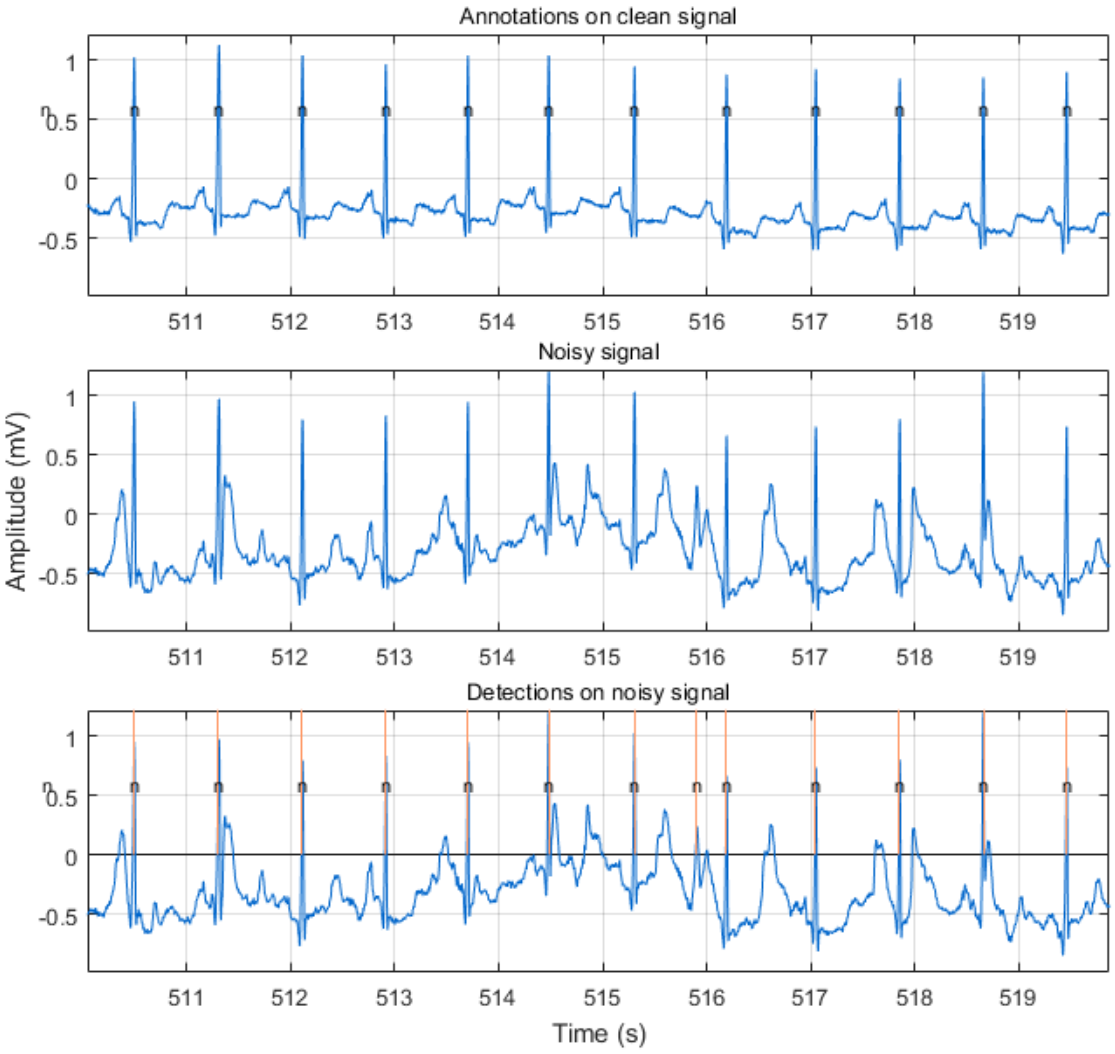

Figure 18: Record 100 clean signal annotated by experts (top) compared to noisy signal annotated by Algorithm 1 (bottom). False positive beat detection at approximately 516 s in the noisy signal.

4.2 Results from the experimental study

Simultaneous ECG and IMU recordings were made while performing four different movements in order to study the relations between movement, ECG movement artifacts, and the IMU signals from several locations. Examples of the ECG and IMU data are visualized in Figures 20–24.

Prior to analysis, the signals had to be synchronized to have as little time-difference as possible. The heel-drop movement that was performed before the actual test movements was found to work well as a reference movement since it caused a strong and relatively sharp peak in all the acceleration recordings, including the acceleration signal recorded by the ECG device itself. The mechanical synchronization signal is visualized in Figure 19. Acceleration signals on the first three rows are from the IMU that was placed above the ECG device. The acceleration signal on the last row

is from the acceleration measurement made by the ECG devices accelerometer. The time axes of the IMU ECG signals were aligned according to the synchronization signal and the time-stamps created by the devices. The IMU signal was found to be 0.65 seconds late compared to the ECG signal and the acceleration signal from the ECG device. However, the accuracy of the time-stamps is unknown and the alignment of the time axes might be lost during longer measurements. Nevertheless, accuracy of mechanical synchronization was found sufficient for the measurements.

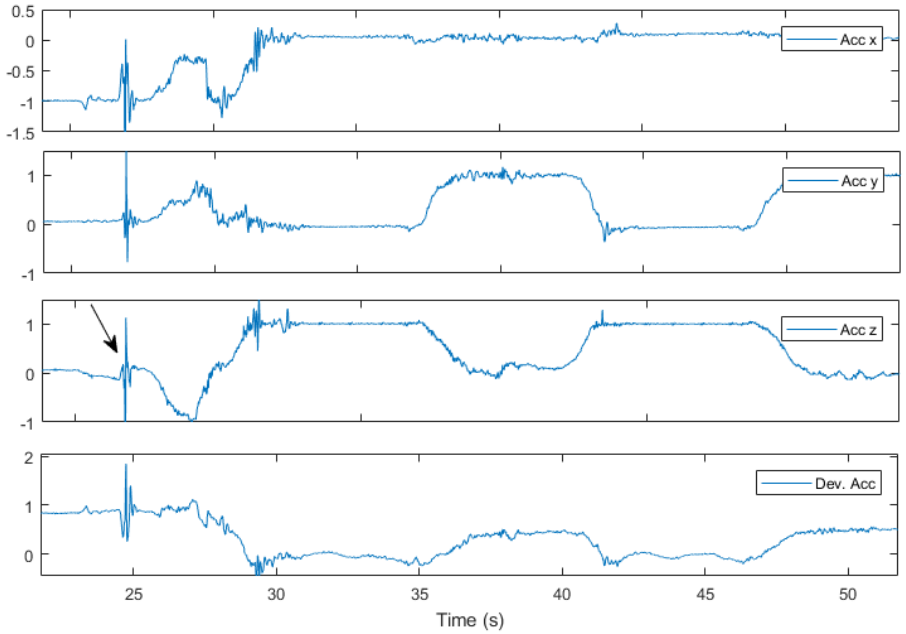

Figure 19: Acceleration data from the IMUs (top) is compared to acceleration data from the ECG device (bottom). The arrow points to the synchronization signal. The first movement, which is rolling from back to side, was performed during the measurement following the synchronization signal.

4.2.1 Correlation between ECG and IMU data

It is hypothesized that the movements inflict distinctive movement artifacts on the ECG signal, and that each ECG channel is affected differently. In order to survey the effects and evaluate which sensors are the most useful, visual and numerical analysis was applied.

Correlation between IMU data and ECG is visualized in Table 5, which includes the sample Pearson correlation coefficients for each ECG channel-IMU channel combination. Average absolute correlation coefficients are clearly different for the movements. The average absolute correlations with the IMU signals for the ECGs recorded during roll and arm movements are higher than the ECGs recorded during wire pull and walking in the stairs. This indicates that ECGs recorded during roll and arm movement recordings are more correlated with the IMU recordings. One possible explanation for higher correlations is a higher level of movement artifacts

caused by these movements, since a clean ECG is not expected to be correlated with the IMU recordings. However, specifically placed accelerometers are capable of picking up the heart rhythm. Another explanation for higher correlations is that the IMUs are placed so that they are capable of picking up specific movements better than others. Accordingly, specific sensor and movement combinations seem to be more highly correlated than the rest. For example, LA and RA acceleration signals are relatively highly correlated with the ECG signal during arm movements. This is an expected result due to the placement of the LA and RA IMUs closer to the upper limbs.

Accelerometer and magnetometer signals are more highly correlated with the ECG signals than the gyroscope signals on average. However, looking only at the averages of the absolute values of correlation reveals only limited information. The gyroscope signals are considerably more correlated with the ECGs measured during rolling from back to side than the other movements. The ECG signals absolute values of correlation with the magnetometer signals are especially low during the wire pull test. This is expected, since the wire pull is such a small movement.

Correlations between the ECG signals and the acceleration signal recorded by the ECG device's own accelerometer are given in Table 6. The acceleration signal is clearly correlated with the ECG Channels 1 and 3 during the first movement, similarly to the acceleration signal in the IMU placed above the ECG device. However, the acceleration signal from the ECG device is more correlated with the wire pull ECG signal compared to the IMU accelerometer's signal. On the other hand, the acceleration signal from the IMU placed above the Faros is more correlated with the arm movement ECG signal. Neither of them is significantly correlated with the staircase ECG. These results make sense, since the IMU does supposedly not move during wire pull, unlike the ECG device. Also, it seems that the ECG device is less affected by the arm movement than the electrodes and IMUs.

Table 5: Correlation between the IMU data and the ECG. Color of each cell corresponds to absolute correlation; the darker the cell, the higher the absolute value of the correlation coefficient. Column-, movement-, row- and sensor means are calculated for absolute values of sample correlation coefficients.

			Roll			Wire pull			Arm movement			Staircase			Row mean	Sensor mean
			1	2	3	1	2	3	1	2	3	1	2	3		
Far	Acc	1	-0,07	0,17	-0,28	0,01	0,04	0,00	0,08	-0,21	-0,05	-0,03	-0,01	0,06	0,09	
		2	-0,44	-0,06	0,46	-0,11	-0,05	-0,08	0,04	0,14	0,42	0,01	-0,02	0,08	0,16	0,15
		3	0,23	0,13	-0,57	0,03	-0,05	-0,06	0,10	-0,61	-0,44	-0,11	0,04	-0,01	0,20	
	Gyro	1	-0,26	-0,14	-0,25	0,00	-0,02	0,05	-0,14	-0,03	-0,07	-0,04	0,09	-0,08	0,10	
		2	0,02	-0,03	-0,05	0,01	0,01	-0,08	-0,09	0,02	-0,02	0,06	0,05	-0,09	0,04	0,07
		3	-0,08	-0,01	-0,18	0,01	-0,03	-0,04	-0,06	-0,04	0,08	-0,05	0,09	0,07	0,06	
	Mag	1	-0,05	-0,18	0,43	-0,05	0,04	0,09	-0,03	0,52	0,28	-0,15	-0,05	0,01	0,16	
		2	0,40	0,04	-0,48	0,08	0,03	0,09	-0,06	-0,18	-0,34	0,53	0,00	-0,07	0,19	0,19
		3	-0,27	-0,10	0,60	-0,04	0,07	0,04	-0,06	0,59	0,47	0,11	-0,09	0,07	0,21	
FLL	Acc	1	-0,06	0,16	-0,39	0,06	0,00	0,05	0,04	-0,21	-0,19	-0,02	0,01	0,03	0,10	
		2	-0,38	-0,10	0,51	-0,02	-0,01	-0,08	0,31	0,36	0,14	0,05	-0,04	0,08	0,17	0,14
		3	-0,24	0,09	-0,27	0,29	0,08	0,12	0,31	-0,07	-0,12	-0,05	0,03	0,07	0,14	
	Gyro	1	-0,26	-0,12	-0,27	-0,02	0,04	-0,03	-0,20	-0,01	-0,02	-0,06	0,08	-0,10	0,10	
		2	-0,04	-0,07	0,02	-0,01	-0,03	0,08	0,24	0,09	-0,10	0,11	0,03	-0,14	0,08	0,08
		3	0,05	-0,02	-0,10	0,02	-0,02	-0,06	-0,25	0,01	0,04	0,07	-0,02	-0,05	0,06	
	Mag	1	-0,01	-0,14	0,48	0,07	-0,02	0,01	-0,14	0,17	0,20	0,21	-0,13	0,03	0,13	
		2	0,32	0,07	-0,55	-0,02	0,09	0,07	-0,44	-0,34	-0,15	0,17	0,06	-0,11	0,20	0,18
		3	-0,03	-0,13	0,56	-0,25	-0,08	-0,17	0,03	0,38	0,34	0,46	-0,05	-0,01	0,21	
LLA	Acc	1	0,18	0,17	-0,52	0,11	0,01	-0,03	0,11	-0,20	-0,39	0,02	0,05	0,05	0,15	
		2	-0,46	-0,06	0,39	0,23	0,00	-0,05	0,16	-0,22	-0,36	0,17	-0,02	0,00	0,18	0,17
		3	0,27	0,11	-0,55	0,24	0,02	-0,06	-0,06	-0,40	-0,39	0,12	0,05	0,05	0,19	
	Gyro	1	-0,26	-0,11	-0,25	-0,03	0,00	0,00	-0,20	-0,02	0,08	-0,05	0,09	-0,07	0,10	
		2	0,02	-0,08	-0,08	-0,03	0,03	0,03	0,09	-0,01	0,01	0,08	0,04	-0,19	0,06	0,08
		3	0,23	0,12	0,08	0,03	-0,07	-0,02	0,38	0,05	-0,01	0,05	-0,06	0,05	0,10	
	Mag	1	-0,18	-0,15	0,53	0,01	-0,01	0,04	0,02	0,32	0,40	0,27	-0,12	0,03	0,17	
		2	0,43	0,04	-0,44	-0,10	0,04	0,00	-0,27	0,14	0,31	0,48	0,02	-0,10	0,20	0,19
		3	-0,34	-0,08	0,56	-0,12	-0,05	0,06	0,45	0,21	-0,07	0,28	-0,06	0,05	0,20	
RRA	Acc	1	0,22	0,17	-0,53	0,17	0,04	-0,09	0,17	-0,17	-0,37	0,04	0,07	-0,12	0,18	
		2	-0,50	-0,04	0,26	0,37	0,07	0,20	-0,26	0,26	0,43	-0,07	-0,04	0,09	0,22	0,20
		3	0,31	0,09	-0,54	0,23	0,06	-0,11	-0,12	-0,36	-0,33	-0,06	-0,08	-0,06	0,20	
	Gyro	1	-0,28	-0,14	-0,28	-0,06	-0,01	-0,03	0,11	-0,01	-0,02	-0,06	0,08	-0,07	0,10	
		2	-0,01	-0,06	-0,14	0,02	0,04	0,04	0,09	-0,07	0,04	0,04	-0,07	-0,09	0,06	0,08
		3	0,15	0,11	0,07	0,03	-0,01	-0,03	-0,26	-0,06	0,06	0,01	-0,08	0,10	0,08	
	Mag	1	-0,21	-0,15	0,55	-0,07	0,03	0,05	-0,27	0,10	0,31	0,14	-0,11	0,07	0,17	
		2	0,44	0,01	-0,36	-0,15	-0,06	-0,11	0,30	-0,20	-0,38	0,52	0,00	-0,07	0,22	0,20
		3	-0,35	-0,06	0,52	0,00	-0,06	0,13	-0,19	0,27	0,38	-0,35	-0,06	0,14	0,21	
Column mean			0,22	0,10	0,36	0,09	0,04	0,06	0,17	0,20	0,22	0,14	0,05	0,07		
Movement mean				0,23			0,06			0,19			0,09			

Table 6: Correlation between the accelerometer data recorded by the ECG device and the ECG. Color of each cell corresponds to absolute correlation; the darker the cell, the higher the absolute value of the correlation coefficient. Row means are calculated for absolute values of sample correlation coefficients.

			Roll			Wire pull			Arm movement			Staircase			Row mean
			1	2	3	1	2	3	1	2	3	1	2	3	
Far dev	Acc	1	-0,11	-0,07	0,54	-0,07	-0,10	-0,25	-0,18	-0,24	-0,26	0,05	0,04	-0,21	0,18
		2	-0,49	-0,09	0,40	0,51	0,02	0,10	0,14	0,14	0,31	0,00	-0,06	-0,05	0,19
		3	-0,37	-0,10	0,49	-0,25	-0,09	-0,30	-0,21	-0,20	-0,29	0,14	0,02	-0,07	0,21

4.2.2 Effect of different movements on ECG signal

Artifact levels were defined also by visual inspection for comparison with the correlation results. The level of movement artifacts for each movement and the three ECG channels can be found in Table 7. The artifact levels were defined by visual inspection from Figure 20. Movement artifact level 1 corresponds to no movement artifacts or very mild noise on the ECG signal. Both levels 2 and 3 have visible artifacts, but level 3 affects the signal quality considerably more. Movement artifact level 4 signifies artifacts that are very strong and can cause the signal to be partially unreadable. R-peaks can be buried under artifacts in level 4.

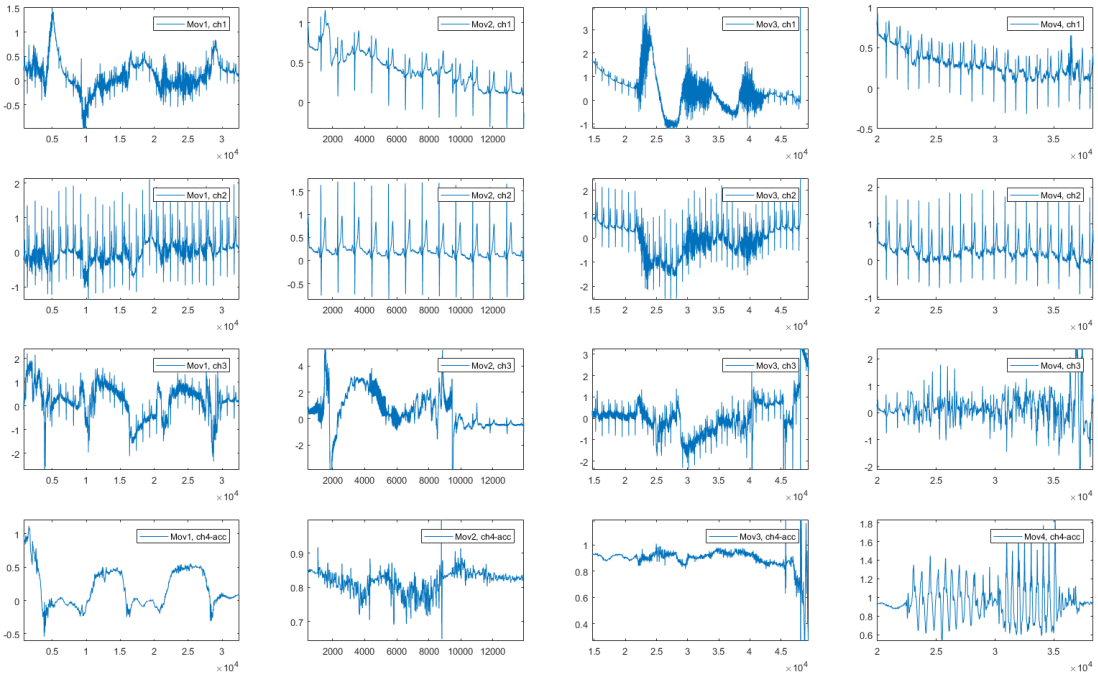

Figure 20: Signals from the ECG devise. ECG channels 1–3 on rows 1–3, accelerometer signal from the ECG device, on row 4, and movements 1–4 on columns 1–4. First movement is rolling from back to stomach, second movement is pulling the ECG wire, third movement is horizontal shoulder rotation, and fourth movement is walking in the stairs.

On average, Channel 3 is the most and Channel 2 the least affected by movement artifacts. This indicates that the ECG channels are affected with different strengths. In addition, effects of the movements are also found distinctive. Rolling from back to side and horizontal rotation of the shoulders cause more severe artifacts than pulling the wire and walking in the stairs on average according to the Table 7.

The effect of movement on the ECG signals is also evaluated by R-peak detection. R-peaks were detected using the Pan-Tompkins algorithm separately from all 3 ECG channels from the four ECG recordings generated in the exploratory study. The amount of false negatives and false positives for each movement and channel can be found in Table 8. Movement artifact levels below 4 do not seem to affect R-peak

detection, even though, for example, T wave detection might be affected. The amount of false positives exceeds the amount of false negatives in most cases, as could be expected based on the simulation results.

Table 7: Movement artifact level defined by visual inspection for each test movement per ECG channel. 1 = Mild noise/none, 2 = Visible artifacts, 3 = Strong artifacts, 4 = Very strong artifacts.

Channel	Movement				
	Roll	Wire Pull	Rotation	Staircase	Mean
1	4	2	4	2	3.00
2	3	1	3	1	2.00
3	3	4	3	4	3.50
Mean	3.33	2.33	3.33	2.33	

Table 8: R-peak detection test on ECG signals recorded during four different movements. FN is the amount of false negatives, FP is the amount of false positives, and R-peaks is the real amount of R-peaks in the ECG records.

Channel	Movement							
	Roll		Wire pull		Rotation		Staircase	
	FN	FP	FN	FP	FN	FP	FN	FP
1	7	29	0	1	18	31	0	0
2	0	0	0	0	0	0	0	0
3	0	8	10	6	1	1	2	16
R-peaks	32		13		27		15	

Turning from back to side caused severe artifacts on all ECG channels, hiding signal features and impairing signal readability. R-peaks are visible on Channels 2 and 3, whereas some QRS complexes are completely buried under the artifacts on Channel 1. Accelerometer, gyroscope, and magnetometer signals from measurement 1 are shown in Figure 21 in addition to the ECG signal from Channel 1. Visual evaluation is in agreement with the higher correlation values for movement 1 in Table 5.

Pulling the ECG wire below the ECG device induced severe artifacts only on ECG Channel 3, whereas Channel 1 has visible artifacts that might obstruct the extraction of other ECG parameters than QRS complexes. Channel 2 has no visible artifacts. The IMU signals from the IMU that was connected above the Faros ECG device are shown in Figure 22 in addition to the ECG signal from Channel 1. The correlation values do not distinct which channel is affected by movement artifacts unlike the visual inspection. Additionally, the Faros accelerometer Channel 2 is quite highly correlated with the ECG Channel 1, which is not evident by visual inspection.

Arm movements generated strong artifacts in the ECG signal, which can be seen in Figure 23. Strong artifacts could be expected from the high correlation values with the IMU signals as well. Channel 1 is unreadable during the movements, but Channels 2 and 3 have visible R-peaks. Other signal components, such as T waves are heavily buried under artifacts on Channels 2 and 3 during the movements in measurement 3. IMU data from the IMU sensor above the ECG device shows some changes during the shoulder horizontal rotations, however checking the data from an IMU that is located further from the midline might show stronger reactions in the accelerometer and gyroscope signals.

ECG and IMU measurements made during walking in the stairs are visualized in Figure 24. Channel 1 has visible artifacts but is easily readable, whereas no artifacts are found during the movement on Channel 2. Channel 3 is heavily affected by the fourth movement, and the R-peaks are only partly visible. Even though Channel 3 is visibly disturbed, the correlation values with the IMU signals are very low. This could indicate that the IMUs did not succeed in capturing the movements caused by walking on the stairs. However, since Channels 1 and 2 were relatively mildly affected by the fourth movement, this might also indicate that the connection on Channel 3 was somehow disturbed. Channel 3 signal had some 50 Hz noise during measurements 1 and 2, which also suggests that Channel 3 was disturbed in a way that was not necessarily related to movement, but most likely power line interference.

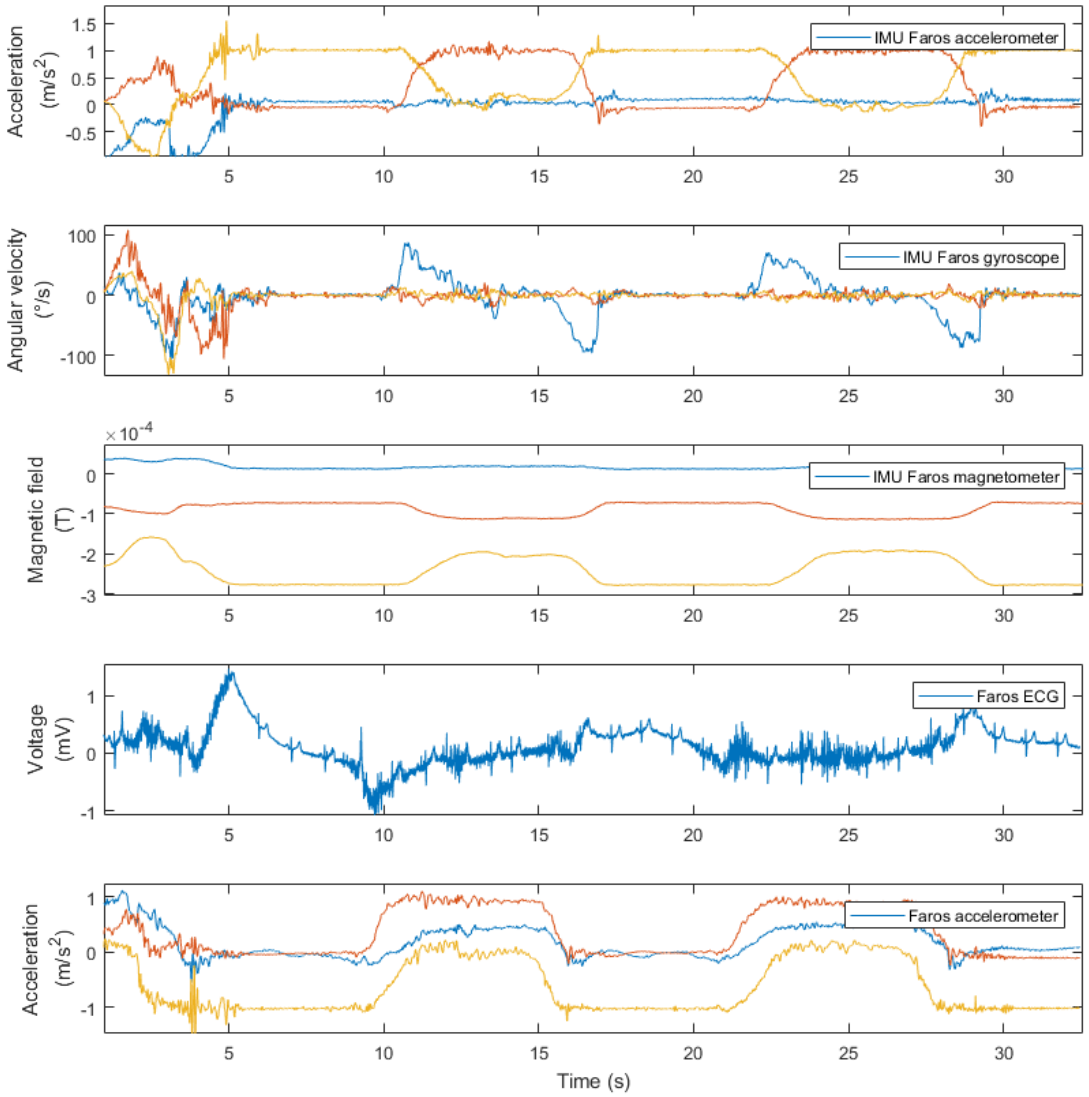

Figure 21: Signals from the IMU (rows 1-3) are compared to the signals from the ECG device (rows 4-5). The first movement, which is turning from back to side, was performed several times during the measurement.

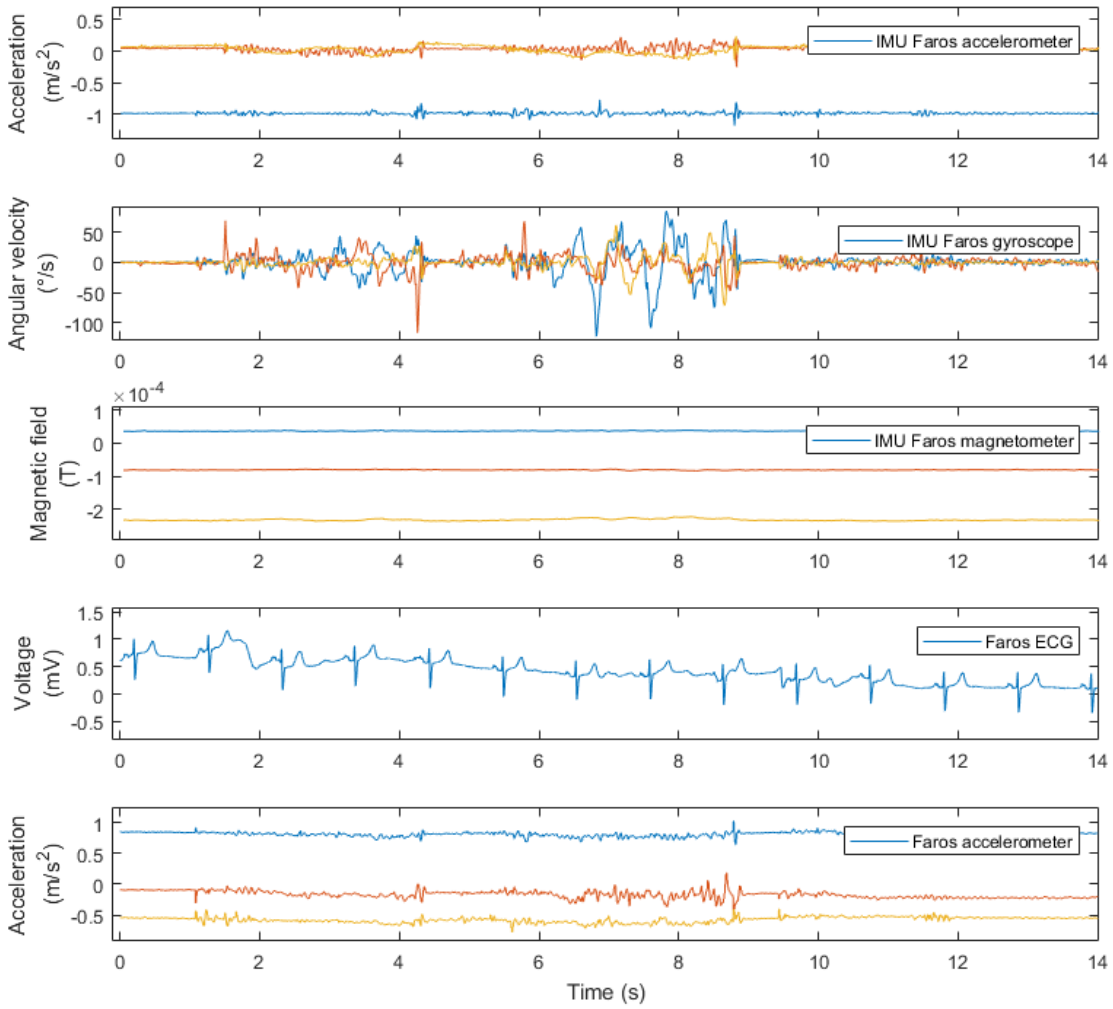

Figure 22: Signals from the IMU (rows 1-3) are compared to the signals from the ECG device (rows 4-5). The second movement, which is pulling the wire of the ECG device, was performed several times during the measurement.

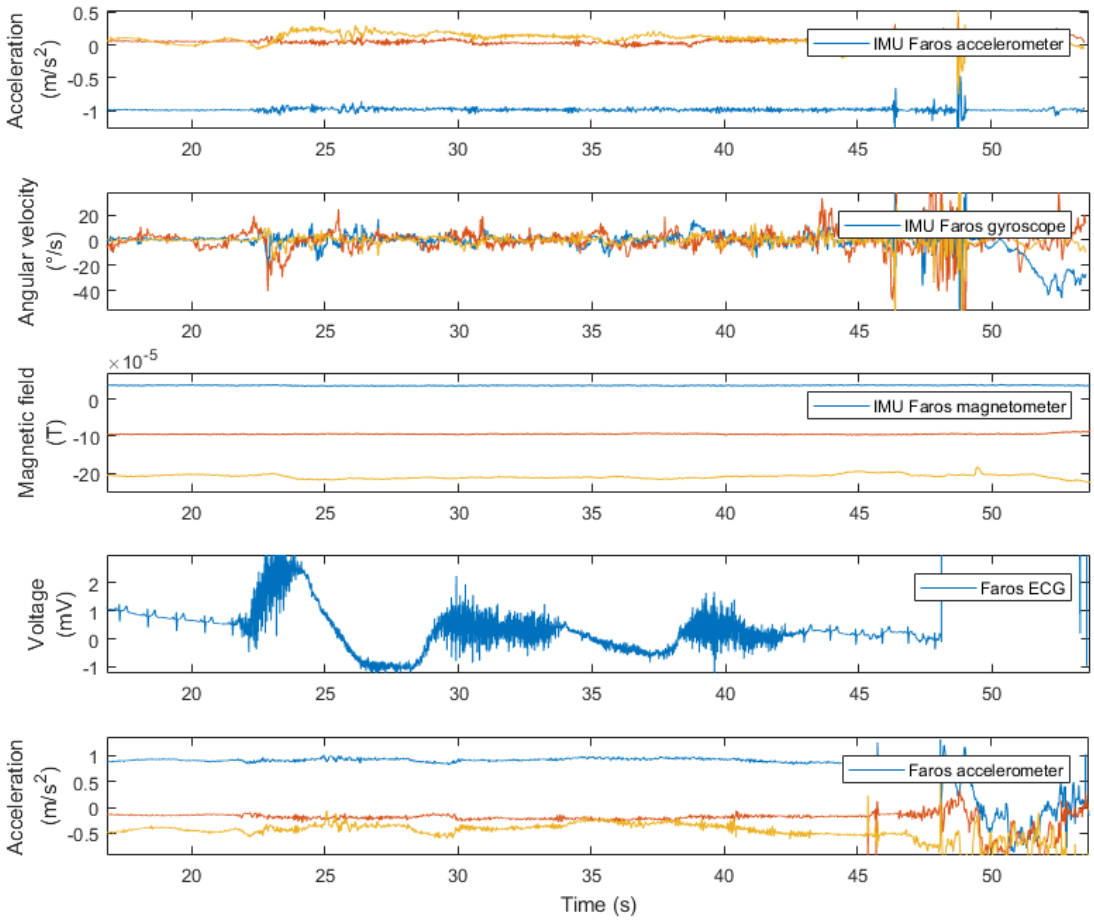

Figure 23: Signals from the IMU (rows 1-3) are compared to the signals from the ECG device (rows 4-5). The third movement, which is shoulder horizontal rotation, was repeated a couple of times during the measurement.

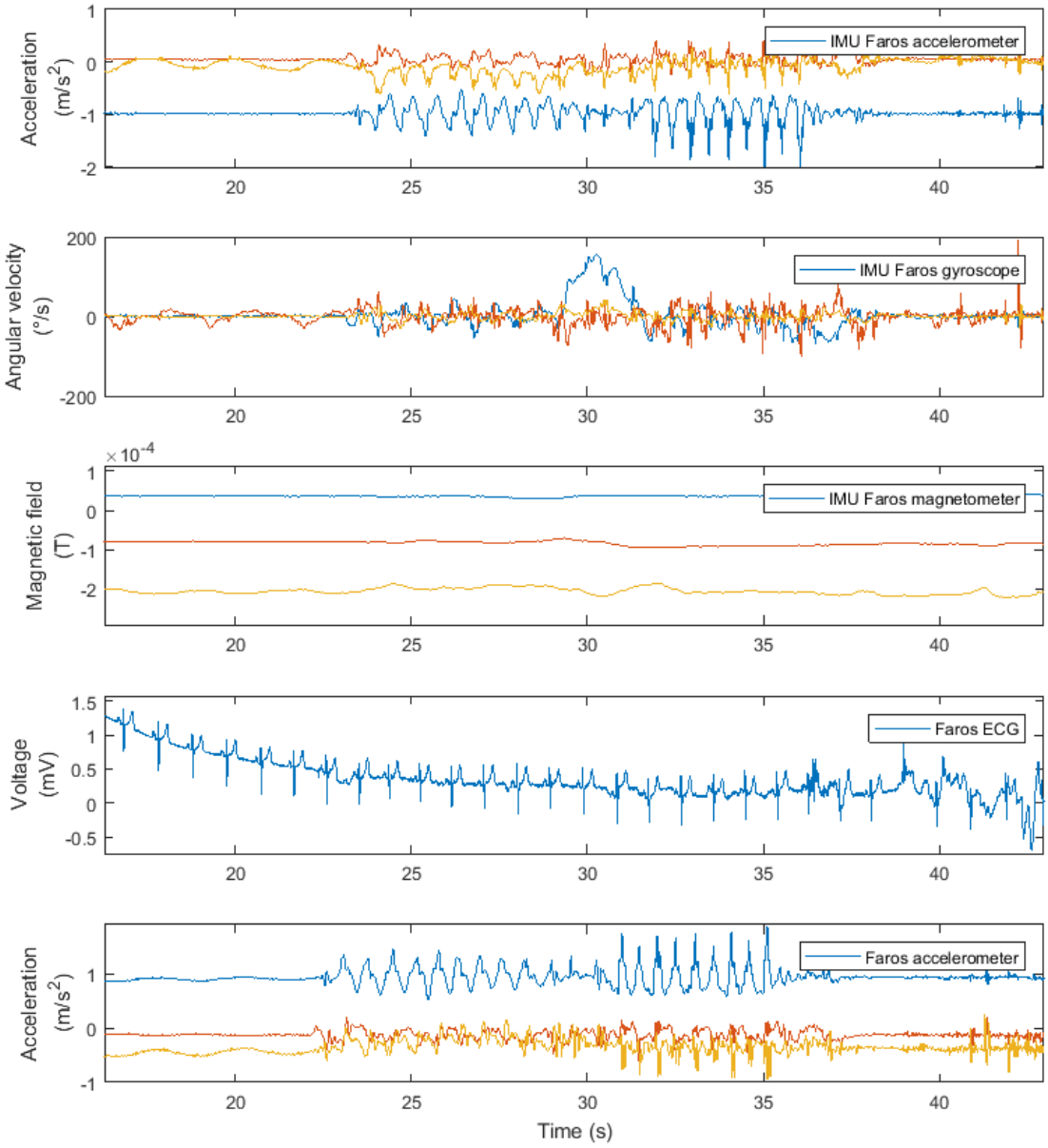

Figure 24: Signals from the IMU (rows 1-3) are compared to the signals from the ECG device (rows 4-5). The fourth movement included that the measurement subject was walking in the staircase during the measurement.

5 Discussion

Critical evaluation of the results and observations made in this thesis is carried out in the following chapters. The results gained in this thesis process are also reflected on the results found in the literature from relevant studies.

5.1 Evaluation of the results from simulations

When comparing the artificially noisy records utilized in the simulation study and the records made in the short experimental study, some differences are found between the simulated and the real movement artifacts. First of all, the movement artifacts seen in the records of the experimental study are more varying due to different movements, and occur at specific times. However, similar shapes occur in simulated and experimental records and so the simulated records seem to resemble reality quite well, as concluded in the illustrative case study. The noise-level in the experimental records is more varying than in the simulated records. Having additional noise levels in the simulation study corresponding to SNRs 3 and 1 as calculated by Equation (7) could be interesting, since the noise in the experimental records gets very high at times. However, the three noise levels utilized in the simulation study are enough to illustrate the effect of noise on QRS-detection and verify that the detection statistics are affected.

The results gained in this research agree with previous studies (Zhang et al., 2016) (Romero et al., 2009). Similar studies have been conducted using different algorithms for specific purposes, such as separating the heart rhythm from ECG that is contaminated by noise and artifacts. Other studies have also concluded that statistics such as sensitivity and specificity have distinct reactions to noise.

Romero et al. (2009) conducted a simulation using record 100 from the MITDB database and the noise record em from the NSTDB database. They used two wavelet based algorithms for R-peak detection in addition to the Pan-Tompkins algorithm. The results agree mostly with the results gained in the simulation study conducted in this thesis. They found that positive predictivity of the two wavelet based algorithms was more affected than sensitivity by increasing the noise level, similarly to the results in this thesis. However, the positive predictivity of the Pan-Tompkins algorithm was found less affected than sensitivity according to their study. The difference might be explained by the different range of noise levels used and the use of only one record. The detection statistics could also have been calculated using alternative parameters, such as window size.

Similar noise robustness studies have also been conducted using varying noise sources, such as CPR related noise. CPR artifacts can be compared to movement artifacts, since both originate from the skin-electrode interface and electrode movement (Fitzgibbon et al., 2002). Zhang et al. (2016) studied the effect of increased noise level on the classification of ventricular fibrillation and sinus rhythm during CPR. All the algorithms that were evaluated in the study lost their specificity at a faster rate than sensitivity as the SNR level decreased. This phenomena is also detected in other studies related to CPR artifact suppression (Werther et al., 2009).

5.2 Evaluation of the results from combined ECG and IMU measurement

Correlation does not reveal causal relationships. However, when combined with visual inspection it can reveal tendencies in the data that might be missed if only visual inspection was conducted. More sophisticated methods are required to get a better understanding of the causal relationship between movement artifacts and IMU data. The test data utilized in this thesis is limited, as it contains only one subject and one recording of each movement set. Accordingly, some findings from this study might be unique to the specific measurement setting. For example, individual cells and small differences in Table 5 can be well affected by chance, and the values can only be taken as guidelines for further studies and other methods. Especially the choice of IMUs and the ECG device itself could have a significant effect on the results if the study was conducted again with different devices.

More measurements should be made with a similar protocol and more test subjects to check the validity of the results. It would be easy to conduct new measurements provided that the measurement equipment is available, since the protocol was simple and short. Some factors that can cause variability between repeated measurements include: exact placement of the electrodes and the IMUs, electrode condition, measurement environment (electrical interference), skin preparation, exact implementation of the movements, and measurement subject's body shape, age, and gender. In order to minimize the effect of electrode placement, skin preparation, and movement implementation, the measurements should be guided by a physician. Additionally, the protocol could be practiced beforehand to make sure that the measurement subject conducts them correctly.

The effect of other factors than movements should be reduced so that the artifacts are more easily linked to specific movements. The movements could be quite reliably connected visually to the artifacts in the ECG signal, however some additional noise occurred especially in Channel 3. A repeated experiment was later executed by the research group to confirm the source of the noise. Linking the movements to the artifacts could be enhanced by, for example, recording the measurements on video. This would be well feasible in small scale studies, but could increase the amount of data unnecessarily in a larger study. Additionally, recognizability of the volunteers should be minimized.

The electrodes can have an effect on the results of the experimental study as movement artifacts arise from the skin-electrode interface. Electrode contact can worsen during longer measurements when using wet electrodes, which has an effect on ECG signal quality. However, the protocol used to produce the data used in this thesis is relatively short, so time will most likely not affect the condition of the electrode contact during the measurements. Sweating is another factor that can affect the electrode contact, however the protocol used to create the experimental data discussed in this thesis should not cause much physical exertion in normal room temperature to patients in good or moderate health. The choice between Ag/AgCl ECG electrodes by different companies has most likely no significant effect on the results.

Only disposable wet electrodes were used in the IMU/ECG study, as they are easily available and are believed to be more resistant to movement artifacts. However, the superiority of wet electrodes over dry electrodes in regard to movement artifacts has been questioned especially when the measurement lasts several days (Searle and Kirkup, 2000). The studies that compare dry electrodes or textile electrodes to wet electrodes during movement have varying results, which is most likely due to great differences between the dry electrodes and dry electrode setups (Marozas et al., 2011).

5.3 Possible improvements

Possible improvements to the simulation study include increasing the amount of noise levels, algorithms, and types of noise added. Furthermore, studying the classification performance under moderate to strong noise would be an interesting method to assess false alarm related problems. Also, the effect of noise should be tested on other databases in addition to the MITDB database to get more reliable results especially when it comes to less common beat types. The reliability of the results related to the effect of noise on the detection probability of different beat types is hindered by the amount of the less common beat types in the database. However, using MITDB makes the results comparable to many other studies in the field.

Another improvement that would be beneficial but is out of the scope of this thesis is creating new noise records during specific movements and repeating the simulations. This would allow one to study which types of movements are more prone to inflict false detections or hide heart beats in the ECG. Studying the effect of different movements using the experimental protocol described in this thesis might be more realistic than simulation, but does not offer the possibility to compare the results to the golden truth annotations that are at hand for open source ECG databases such as the MITDB.

Possible improvements to the combined ECG and IMU measurements include more test subjects, more repetitions of each movement, more movements and using an increased amount of IMUs in varying locations. Especially in order to find the optimal combination of IMU sensors, their placement should be reconsidered based on previous results. The IMU sensor that was placed above the R/RA electrode as shown in Figure 14 has the highest average absolute correlation of the IMU sensors with the ECG signals, and so the placement could be used in future studies. The acceleration signal recorded by the ECG device appears more correlated with the wire pull ECG than the R/RA acceleration signal, however, the difference is not necessarily significant. More experiments should be made in order to find the best candidate to be used as a movement reference IMU placement to recognize artifacts that are caused by wire pull-like movements. One option to consider is try placing one IMU below the ECG device. It could be better to monitor the movement of the leads directly. However, this might not be feasible due to the size of the IMUs used to produce the data described in the thesis.

The IMU sensor data could be used for either signal enhancement or producing a signal quality index when the placement of the IMUs has been set so that they are able

to capture the movements that are most likely to cause movement artifacts. According to this study, movement artifacts are most likely to be caused by movements that affect the chest area, where the electrodes are also placed. Movements that affect the chest area include, for example, rolling from back to side or shoulder rotation. The placement of the IMU could also be optimized depending on the ECG channel that is recorded. Additionally, the data from different IMU sensor types, namely the accelerometer, gyroscope, and magnetometer should be fused in order to produce a better movement reference.

6 Conclusions

ECG is used to measure the electrical activity of the heart from the outside of the patients body. ECG is commonly measured using a varying amount of Ag/AgCl electrodes and leads that capture voltage changes. Heart beats are captured as a repeating waveform, that consists of the P and T waves and the QRS complex. Abnormalities in the signal are observed to diagnose the patient. Deviations from the standard P-QRS-T waveform can be seen in the electrocardiograph as irregular peak shapes, intervals, or missing peaks.

Computational ECG analysis is used to process ECG signals and to make automated diagnoses to aid medical practitioners. The main steps in analysis are signal conversion into digital format, noise removal, R-peak detection, and wave delineation. These steps might be followed by more advanced analysis such as beat type classification. Machine learning methods are typically applied in the advanced analysis steps. Signal quality restricts the applicability of advanced analysis similarly as it restricts the physicians analysis. Noise and artifacts in the signal can make the signal unreadable or hide important elements. Bad signal quality can also cause false alarms, which is a severe problem in hospital monitoring systems. Therefore, the importance of both signal quality enhancement and signal quality monitoring is emphasized.

Even though most ECG recordings are made in hospitals, the increase of remote health care inflicts new requirements on ECG recording devices and signal processing. Ambulatory ECG recordings are subject to severe and varying noise, so traditional signal processing methods might not be sufficient to reach desirable signal quality. Furthermore, the number of leads that can be used is typically very restricted. Movement artifacts are demanding to separate from the signal of the heart not only because of their variability and unpredictability, but also because the frequency spectra of P-QRS-T and movement artifacts overlap. Additionally, powerful signal processing methods designed to remove noise might distort the ECG signal and hide small details that are used for diagnosis.

QRS complex detection positive predictivity is especially affected by gradually increasing movement artifact levels according to the simulation study conducted in this thesis. Also the QRS complex detection sensitivity lowers as the noise level increases according to the results. The relationship between beat type and correct detection probability was inspected based on the simulation results. As could be expected, normal beats were easier to detect than, for example, PVCs according to the results. However, the algorithms were not specifically designed to detect arrhythmic beats, which obviously effects their performance. Furthermore, majority of the false detections made could have been due to the similarity between movement artifacts and PVC waveform.

In order to separate movement artifacts from the ECG records various approaches have been taken in the literature. For example, adaptive filtering utilizes knowledge from additional sensors. Additional sensors are used to capture movement of the electrodes or the measurement subject in order to capture reference noise signals for adaptive noise removal algorithms. Variables such as acceleration, pressure, distance,

and impedance have been measured using additional sensors during ECG.

Recordings made by a system that captures movement using several inertial measurement units simultaneously to an ECG recording were studied in this thesis. Stretching of the skin causes movement artifacts, and so capturing the relative movement of the electrode and the skin surrounding the electrode could be beneficial in modeling the artifact. The ability to capture movements that are behind the movement artifacts in the ECG was studied in a small scale laboratory experiment. An IMU was connected above each ECG electrode to study the effect of IMU placement. Four different movements were performed during an ECG recording in order to induce movement related noise to the signal. The IMU signal was inspected visually and correlated with the ECG signal to evaluate the setup and find a starting point for further studies.

Rolling from back to side and arm movements were found to be better correlated with the IMU signals and cause more severe artifacts to the ECG signal. Additionally, specific IMU locations were found especially good in capturing specific movements compared to others. RRA was found to be the most correlated with the ECG signal in general, however looking at the correlation alone is not sufficient. Wire pull was not well captured by the IMUs and new locations for the sensors should be experimented to achieve a movement reference for possible wire pull related movement artifacts.

References

Abdelazez, M., Quesnel, P. X., Chan, A. D., and Yang, H. (2017). Signal quality analysis of ambulatory electrocardiograms to gate false myocardial ischemia alarms. *IEEE Transactions on Biomedical Engineering*, 64(6):1318–1325.

Addison, P. (2005). Wavelet transforms and the ECG: A review. *Physiological Measurement*, 26(5):R155–R199.

Afonso, V. X. (1993). ECG QRS detection. In Tompkins, W. J., editor, *Biomedical Digital Signal Processing: C Language Examples and Laboratory Experiments for the IBM PC*, chapter 12, pages 237–264. Englewood Cliffs, NJ: Prentice-Hall.

Afonso, V. X., Tompkins, W. J., Nguyen, T. Q., and Luo, S. (1999). ECG beat detection using filter banks. *IEEE Transactions on Biomedical Engineering*, 46(2):192–202.

AlGhatrif, M. and Lindsay, J. (2011). A brief review: History to understand fundamentals of electrocardiography. *Journal of Community Hospital Internal Medicine Perspectives*, 2(1):1–5.

American Heart Association (1967). Report of committee on electrocardiography. Recommendations for standardization of leads and of specifications for instruments in electrocardiography and vectorcardiography. *Circulation*, 35(3):583–602.

Andreao, R. V., Dorizzi, B., and Boudy, J. (2006). ECG signal analysis through hidden Markov models. *IEEE Transactions on Biomedical Engineering*, 53(8):1541–1549.

Antzelevitch, C. and Burashnikov, A. (2011). Overview of basic mechanisms of cardiac arrhythmia. *Cardiac electrophysiology clinics*, 3(1):23–45.

Arzeno, N. M., Deng, Z.-D., and Poon, C.-S. (2008). Analysis of first-derivative based QRS detection algorithms. *IEEE Transactions on Biomedical Engineering*, 55(2):478–484.

Baig, M. M., Gholamhosseini, H., and Connolly, M. J. (2013). A comprehensive survey of wearable and wireless ECG monitoring systems for older adults. *Medical & Biological Engineering & Computing*, 51(5):485–495.

Bailey, J., Berson, A., Garson Jr., A., Horan, L., Macfarlane, P., Mortara, D., and Zywietz, C. (1990). Recommendations for standardization and specifications in automated electrocardiography: Bandwidth and digital signal processing. *Circulation*, 81(2):730–739.

Barold, S. (2003). Willem Einthoven and the birth of clinical electrocardiography a hundred years ago. *Cardiac Electrophysiology Review*, 7(99):99–104.

Bates, J. (2012). Linear systems and the 1-D Fourier transform. In Peters, T. M. and Williams, J. C., editors, *Fourier Transform in Biomedical Engineering*. Birkhauser Boston.

Behar, J., Oster, J., Li, Q., and Clifford, G. D. (2013). ECG signal quality during arrhythmia and its application to false alarm reduction. *IEEE Transactions on Biomedical Engineering*, 60(6):1660–1666.

Bentley, P. M. and McDonnell, J. T. E. (1994). Wavelet transforms: An introduction. *Electronics Communication Engineering Journal*, 6(4):175–186.

Berger, R. D., Palazzolo, J., and Halperin, H. (2007). Rhythm discrimination during uninterrupted CPR using motion artifact reduction system. *Resuscitation*, 75(1):145–152.

Bhargava, V. and Goldberger, A. (1981). Myocardial infarction diminishes both low and high frequency QRS potentials: Power spectrum analysis of lead II. *Journal of Electrocardiology*, 14(1):57–60.

Burch, G. E. and DePasquale, N. P. (1990). *A history of electrocardiography*. Norman Publishing. pages 25–35.

Buxi, D., Kim, S., Van Helleputte, N., Altini, M., Wijsman, J., Yazicioglu, R. F., Penders, J., and Van Hoof, C. (2012). Correlation between electrode-tissue impedance and motion artifact in biopotential recordings. *IEEE Sensors Journal*, 12:3373–3383.

Ceylan, R., Özbay, Y., and Karlik, B. (2009). A novel approach for classification of ECG arrhythmias: Type-2 fuzzy clustering neural network. *Expert Systems with Applications*, 36(3, Part 2):6721–6726.

Chung, W.-Y., Lee, Y.-D., and Jung, S.-J. (2008). A wireless sensor network compatible wearable u-healthcare monitoring system using integrated ECG, accelerometer and SpO2. In *30th Annual International Conference of the IEEE Engineering in Medicine and Biology Society*, pages 1529–1532. IEEE.

Clifford, G. D. (2006). Advanced methods and tools for ECG data analysis. In Gari D. Clifford, F. A. and McSharry., P. E., editors, *ECG Statistics, Noise, Artifacts, and Missing Data*, chapter 3, pages 55–100. Artech House.

Crawford, J. and Doherty, L. (2011). *Practical aspects of ECG recording*. M&K Update Ltd. pages 33–36.

Cvach, M. (2012). Monitor alarm fatigue: An integrative review. *Biomedical Instrumentation & Technology*, 46(4):268–277.

De Lannoy, G., Frenay, B., Verleysen, M., and Delbeke, J. (2009). Supervised ECG delineation using the wavelet transform and hidden Markov models. In *4th European Conference of the International Federation for Medical and Biological Engineering*, pages 22–25. Springer Berlin Heidelberg.

El-Dahshan, E.-S. A. (2011). Genetic algorithm and wavelet hybrid scheme for ECG signal denoising. *Telecommunication Systems*, 46(3):209–215.

Fitzgibbon, E., Berger, R., Tsitlik, J., and Halperin, H. (2002). Determination of the noise source in the electrocardiogram during cardiopulmonary resuscitation. *Critical Care Medicine*, 30(4 Supplement):S148–S153.

Forner-Cordero, A., Mateu-Arce, M., Forner-Cordero, I., Alcántara, E., Moreno, J., and Pons, J. (2008). Study of the motion artefacts of skin-mounted inertial sensors under different attachment conditions. *Physiological measurement*, 29(4):N21.

Forvi, E., Bedoni, M., Carabalona, R., Soncini, M., Mazzoleni, P., Rizzo, F., O'Mahony, C., Morasso, C., Cassarà, D., and Gramatica, F. (2012). Preliminary technological assessment of microneedles-based dry electrodes for biopotential monitoring in clinical examinations. *Sensors and Actuators, A: Physical*, 180:177–186.

Gacek, A. (2011). An introduction to ECG signal processing and analysis. In Gacek, A. and Pedrycz, W., editors, *ECG Signal Processing, Classification and Interpretation*, chapter 2, pages 21–46. Springer.

Geddes, L. A. and Hoff, H. E. (1971). The discovery of bioelectricity and current electricity the Galvani-Volta controversy. *IEEE Spectrum*, 8(12):38–46.

Gholam-Hosseini, H., Nazeran, H., and Reynolds, K. J. (1998). ECG noise cancellation using digital filters. In *Proceedings of the 2nd International Conference on Bioelectromagnetism*, pages 151–152. IEEE.

Goldberger, A. L., Amaral, L. A., Glass, L., Hausdorff, J. M., Ivanov, P. C., Mark, R. G., Mietus, J. E., Moody, G. B., Peng, C.-K., and Stanley, H. E. (2000). Physiobank, Physiotoolkit, and Physionet. *Circulation*, 101(23):e215–e220.

Goy, J.-J., Staufer, J.-C., Schlaepfer, J., and Christeler, P. (2013). *Electrocardiography (ECG)*. Bentham Science Publishers.

Hamilton, P., Curley, M., Aimi, R., and Sae-Hau, C. (2000). Comparison of methods for adaptive removal of motion artifact. In *Computers in Cardiology Conference*, volume 27, pages 383–386. IEEE.

Hamilton, P. S. and Curley, M. G. (1997). Adaptive removal of motion artifact. In *Proceedings of the 19th Annual International Conference of the IEEE Engineering in Medicine and Biology Society*, volume 1, pages 297–299. IEEE.

Holbrook, K. A. and Odland, G. F. (1974). Regional differences in the thickness (cell layers) of the human stratum corneum: An ultrastructural analysis. *Journal of Investigative Dermatology*, 62(4):415–422.

Jabaudon, D., Sztajzel, J., Sievert, K., Landis, T., and Sztajzel, R. (2004). Usefulness of ambulatory 7-day ECG monitoring for the detection of atrial fibrillation and flutter after acute stroke and transient ischemic attack. *Stroke*, 35(7):1647–1651.

Jambukia, S. H., Dabhi, V. K., and Prajapati, H. B. (2015). Classification of ECG signals using machine learning techniques: A survey. In *International Conference on Advances in Computer Engineering and Applications*, pages 714–721. IEEE.

Jean-Jacques, B., De Roy, L., Mansourati, J., Poezevara, Y., Marcon, J.-L., Schoels, W., Hidden-Lucet, F., and Barnay, C. (2004). Atrial pacing for prevention of atrial fibrillation: Assessment of simultaneously implemented algorithms. *EP Europace*, 6(5):371.

Jiang, X., Zhang, L., Zhao, Q., and Albayrak, S. (2006). ECG arrhythmias recognition system based on independent component analysis feature extraction. In *TENCON 2006. IEEE Region 10 Conference*, pages 1–4. IEEE.

Jung, H.-K. and Jeong, D.-U. (2012). Development of wearable ECG measurement system using EMD for motion artifact removal. In *7th International Conference on Computing and Convergence Technology*, pages 299–304. IEEE.

Kashani, A. and Barold, S. S. (2005). Significance of QRS complex duration in patients with heart failure. *Journal of the American College of Cardiology*, 46(12):2183–2192.

Katz, A. (2010). *Physiology of the Heart*. Lippincott Williams and Wilkins.

Kemp, B., Värri, A., Rosa, A. C., Nielsen, K. D., and Gade, J. (1992). A simple format for exchange of digitized polygraphic recordings. *Electroencephalography and clinical neurophysiology*, 82(5):391–393.

Khurana, I. (2005). *Textbook Of Medical Physiology*. Elsevier.

Kim, Y. and Tewfik, A. H. (2015). A novel QRS complex detection on ECG with motion artifact during exercise. In *International Conference on Acoustics, Speech and Signal Processing*, pages 972–976. IEEE.

Kirst, M., Glauner, B., and Ottenbacher, J. (2011). Using DWT for ECG motion artifact reduction with noise-correlating signals. In *Annual International Conference of the IEEE Engineering in Medicine and Biology Society*, pages 4804–4807. IEEE.

Kishimoto, Y., Kutsuna, Y., and Oguri, K. (2007). Detecting motion artifact ECG noise during sleeping by means of a tri-axis accelerometer. In *29th Annual International Conference of the IEEE Engineering in Medicine and Biology Society*, pages 2669–2672. IEEE.

Kit, C., Chan, A., Hamada, H., Higuchi, K., and Maenaka, K. (2013). Adhesive plaster-type human activity monitoring device. *Transactions of Japanese Society for Medical and Biological Engineering*, 51(Supplement):M–158.

Kitazaki, S. and Griffin, M. J. (1995). A data correction method for surface measurement of vibration on the human body. *Journal of Biomechanics*, 28(7):885–890.

Kohler, B. U., Hennig, C., and Orglmeister, R. (2002). The principles of software QRS detection. *IEEE Engineering in Medicine and Biology Magazine*, 21(1):42–57.

Koivisto, T., Pänkäälä, M., Hurnanen, T., Vasankari, T., Kiviniemi, T., Saraste, A., and Airaksinen, J. (2015). Automatic detection of atrial fibrillation using MEMS accelerometer. In *Computing in Cardiology Conference*, pages 829–832. IEEE.

Lüderitz, B. (2003). Augustus Desiré Waller (1856–1922)—The first to record the electrical activity of the human heart. *Journal of Interventional Cardiac Electrophysiology*, 9(1):59–60.

Lear, S. A., Brozic, A., Myers, J. N., and Ignaszewski, A. (1999). Exercise stress testing. *Sports Medicine*, 27(5):285–312.

Li, C., Zheng, C., and Tai, C. (1995). Detection of ECG characteristic points using wavelet transforms. *IEEE Transactions on Biomedical Engineering*, 42(1):21–28.

Li, Q., Rajagopalan, C., and Clifford, G. D. (2014). A machine learning approach to multi-level ECG signal quality classification. *Computer methods and programs in biomedicine*, 117(3):435–447.

Liu, S.-H. (2011). Motion artifact reduction in electrocardiogram using adaptive filter. *Journal of Medical and Biological Engineering*, 31(1):67–72.

Liu, Y. and Pecht, M. G. (2006). Reduction of skin stretch induced motion artifacts in electrocardiogram monitoring using adaptive filtering. In *28th Annual International Conference of the IEEE Engineering in Medicine and Biology Society*, pages 6045–6048. IEEE.

Lönnblad, J., Nilsson, G., Folke, M., Hök, B., Lindén, M., and Bäcklund, Y. (2005). Artefacts in continuous ECG recordings–provoking and preventing manoeuvres. *Scandinavian Cardiovascular Journal*, 39(3):167–171.

Ma, L. K., Ma, P. T. S., and Leung, A. K. C. (2009). Ventricular flutter and fibrillation. In Lang, F., editor, *Encyclopedia of Molecular Mechanisms of Disease*, pages 2188–2189. Springer Berlin Heidelberg.

Mallat, S. and Hwang, W. (1992). Singularity detection and processing with wavelets. *IEEE Transactions on Information Theory*, 38(2):617–643.

Mar, T., Zaunseder, S., Martínez, J., Llamedo, M., and Poll, R. (2011). Optimization of ECG classification by means of feature selection. *IEEE Transactions on Biomedical Engineering*, 58(8):2168–2177.

Marozas, V., Petrenas, A., Daukantas, S., and Lukosevicius, A. (2011). A comparison of conductive textile-based and silver/silver chloride gel electrodes in exercise electrocardiogram recordings. *Journal of Electrocardiology*, 44(2):189–194.

Martis, R. J., Acharya, U. R., and Adeli, H. (2014). Current methods in electrocardiogram characterization. *Computers in Biology and Medicine*, 48:133 – 149.

Martis, R. J., Acharya, U. R., and Min, L. C. (2013). ECG beat classification using PCA, LDA, ICA and discrete wavelet transform. *Biomedical Signal Processing and Control*, 8(5):437 – 448.

MathWorks, Inc. (2017a). MATLAB and Wavelet Toolbox Release 2017a.

MathWorks, Inc. (2017b). MATLAB Release 2017a, Documentation, Root-mean-square level.

McGinnis, R. S., Patel, S., Silva, I., Mahadevan, N., DiCristofaro, S., Jortberg, E., Ceruolo, M., and Aranyosi, A. (2016). Skin mounted accelerometer system for measuring knee range of motion. In *38th Annual International Conference of the Engineering in Medicine and Biology Society*, pages 5298–5302. IEEE.

Milanesi, M., Martini, N., Vanello, N., Positano, V., Santarelli, M., Paradiso, R., De Rossi, D., and Landini, L. (2006). Multichannel techniques for motion artifacts removal from electrocardiographic signals. In *28th Annual International Conference of the IEEE Engineering in Medicine and Biology Society*, pages 3391–3394. IEEE.

Mithun, P., Pandey, P. C., Sebastian, T., Mishra, P., and Pandey, V. K. (2011). A wavelet based technique for suppression of EMG noise and motion artifact in ambulatory ECG. In *Annual International Conference of the IEEE Engineering in Medicine and Biology Society*, pages 7087–7090. IEEE.

Mäntykangas, M. (2016). Improving respiratory rate estimation by combining information from impedance pneumography and electrocardiography. Master's thesis, Aalto University.

Moody, G. (2015). WFDB applications guide. Accessed: 2017-08-04.

Moody, G. B. and Mark, R. G. (2001). The impact of the MIT-BIH arrhythmia database. *IEEE Engineering in Medicine and Biology Magazine*, 20(3):45–50.

Moody, G. B., Muldrow, W., and Mark, R. G. (1984). A noise stress test for arrhythmia detectors. *Computers in Cardiology*, 11(3):381–384.

Moreau, D., Stockslager, J. L., Cheli, R., and Haworth, K., editors (2002). *Lippincott professional guides : Anatomy & Physiology.* Wolters Kluwer Health.

Murphy, K. P. (2012). *Machine Learning: A Probabilistic Perspective.* The MIT Press.

Neuman, M. (2009a). Biopotential amplifiers. In Webster, J. G., editor, *Medical Instrumentation: Application and Design*. John Wiley & Sons, Inc., 4th edition.

Neuman, M. (2009b). Biopotential electrodes. In Webster, J. G., editor, *Medical Instrumentation: Application and Design*. John Wiley & Sons, Inc., 4th edition.

Okamoto, Y. and Mashima, S. (1998). The zero potential and Wilson's central terminal in electrocardiography. *Bioelectrochemistry and Bioenergetics*, 47(2):291–295.

Pal, S. and Mitra, M. (2010). Detection of ECG characteristic points using multiresolution wavelet analysis based selective coefficient method. *Measurement*, 43(2):255–261.

Palaniappan, R. and Khoon, T. E. (2004). Uni-channel PCA for noise reduction from ECG signals. In *Proceedings of the 1st International Bioengineering Conference*, pages 436–439.

Pan, J. and Tompkins, W. (1985). A real-time QRS detection algorithm. *IEEE Transactions on Biomedical Engineering*, BME-32(3):230–236.

Pandia, K., Ravindran, S., Cole, R., Kovacs, G., and Giovangrandi, L. (2010). Motion artifact cancellation to obtain heart sounds from a single chest-worn accelerometer. In *2010 IEEE International Conference on Acoustics, Speech and Signal Processing*, pages 590–593.

Pawar, T., Anantakrishnan, N., Chaudhuri, S., and Duttagupta, S. (2007). Transition detection in body movement activities for wearable ECG. *IEEE Transactions on Biomedical Engineering*, 54(6):1149–1152.

Pengjun, X., Xiaoming, T., and Shanyuan, W. (2011). Measurement of wearable electrode and skin mechanical interaction using displacement and pressure sensors. In *4th International Conference on Biomedical Engineering and Informatics*, volume 2, pages 1131–1134. IEEE.

Poli, R., Cagnoni, S., and Valli, G. (1995). Genetic design of optimum linear and nonlinear QRS detectors. *IEEE Transactions on Biomedical Engineering*, 42(11):1137–1141.

Prasad, G. K. and Sahambi, J. S. (2003). Classification of ECG arrhythmias using multi-resolution analysis and neural networks. In *TENCON 2003. Conference on Convergent Technologies for Asia-Pacific Region*, volume 1, pages 227–231 Vol.1.

Preece, S. J., Goulermas, J. Y., Kenney, L. P., Howard, D., Meijer, K., and Crompton, R. (2009). Activity identification using body-mounted sensors–a review of classification techniques. *Physiological measurement*, 30(4):R1–R33.

Rangayyan, R. M. (2002). *Biomedical Signal Analysis*, volume 33. Wiley India.

Raya, M. A. D. and Sison, L. G. (2002). Adaptive noise cancelling of motion artifact in stress ECG signals using accelerometer. In *Conference Proceedings of the Second Joint EMBS-BMES Conference.*, volume 2, pages 1756–1757. IEEE.

Redmond, S. J., Xie, Y., Chang, D., Basilakis, J., and Lovell, N. H. (2012). Electrocardiogram signal quality measures for unsupervised telehealth environments. *Physiological Measurement*, 33(9):1517–1533.

Romero, I., Berset, T., Buxi, D., Brown, L., Penders, J., Kim, S., Van Helleputte, N., Kim, H., Van Hoof, C., and Yazicioglu, F. (2011). Motion artifact reduction in ambulatory ECG monitoring: An integrated system approach. In *Proceedings of the 2nd Conference on Wireless Health*, pages 1–8. ACM.

Romero, I., Geng, D., and Berset, T. (2012). Adaptive filtering in ECG denoising: A comparative study. In *Computing in Cardiology Conference*, pages 45–48. IEEE.

Romero, I., Grundlehner, B., and Penders, J. (2009). Robust beat detector for ambulatory cardiac monitoring. In *Annual International Conference of the IEEE Engineering in Medicine and Biology Society*, pages 950–953. IEEE.

Ruiz de Gauna, S., Irusta, U., Ruiz, J., Ayala, U., Aramendi, E., and Eftestøl, T. (2014). Rhythm analysis during cardiopulmonary resuscitation: Past, present, and future. *BioMed research international*, 2014:1–13.

Schröder, K., Wegscheider, K., Zeymer, U., Tebbe, U., and Schröder, R. (2001). Extent of ST-segment deviation in a single electrocardiogram lead 90 min after thrombolysis as a predictor of medium-term mortality in acute myocardial infarction. *The Lancet*, 358(9292):1479–1486.

Searle, A. and Kirkup, L. (2000). A direct comparison of wet, dry and insulating bioelectric recording electrodes. *Physiological Measurement*, 21(2):271.

Sedghamiz, H. (2014). Matlab implementation of Pan Tompkins ECG QRS detector. https://www.researchgate.net/publication/313673153_Matlab_Implementation_of_Pan_Tompkins_ECG_QRS_detector. Retrieved August 9, 2017.

Selva (2011). R-peak detection using DWT and classification of arrhythmia using bayesian classifier. https://se.mathworks.com/matlabcentral/fileexchange/32214-r-peak-detection-using-dwt-and-classification-of-arrhythmia-using-bayesian-classifier. Retrieved August 10, 2017.

Semmlow, J. L. (2009). *Biosignal and Medical Image Processing*. CRC Press, 2nd edition.

Silva, I. and Moody, G. B. (2014). An open-source toolbox for analysing and processing Physionet databases in MATLAB and Octave. *Journal of Open Research Software*, 2(1).

Singh, S. and Yadav, K. (2010). Performance evaluation of different adaptive filters for ECG signal processing. *International Journal on Computer Science and Engineering*, 02(05):1880–1883.

Łęski, J. M. and Henzel, N. (2005). ECG baseline wander and powerline interference reduction using nonlinear filter bank. *Signal Processing*, 85(4):781 – 793.

Sörnmo, L. and Laguna, P. (2005). *Bioelectrical Signal Processing in Cardiac and Neurological Applications*. Elsevier Science.

Strasser, F., Muma, M., and Zoubir, A. M. (2012). Motion artifact removal in ECG signals using multi-resolution thresholding. In *Proceedings of the 20th European Signal Processing Conference*, pages 899–903.

Takla, G., Petre, J., Doyle, D., Horibe, M., and Gopakumaran, B. (2006). The problem of artifacts in patient monitor data during surgery: A clinical and methodological review. *Anesthesia and Analgesia*, 103(5):1196–1204.

Tam, H. and Webster, J. (1977). Minimizing electrode motion artifact by skin abrasion. *IEEE Transactions on Biomedical Engineering*, BME-24(2):134–139.

Thakor, N. V., Webster, J. G., and Tompkins, W. J. (1984). Estimation of QRS complex power spectra for design of a QRS filter. *IEEE Transactions on Biomedical Engineering*, (11):702–706.

Thaler, M. S. (2015). *The Only EKG Book You'll Ever Need*. Lippincott Williams&Wilkins, 8th edition.

Tong, D., Bartels, K., and Honeyager, K. (2002). Adaptive reduction of motion artifact in the electrocardiogram. In *Proceedings of the Second Joint EMBS/BMES Conference*, volume 2, pages 1403–1404. IEEE.

Tsutsumi, T., Okamoto, Y., Kubota-Takano, N., Wakatsuki, D., Suzuki, H., Sezaki, K., Iwasawa, K., and Nakajima, T. (2014). Time–frequency analysis of the QRS complex in patients with ischemic cardiomyopathy and myocardial infarction. *International Journal of Cardiology Heart & Vessels*, 4:177–187.

Van Helleputte, N., Konijnenburg, M., Pettine, J., Jee, D.-W., Kim, H., Morgado, A., Van Wegberg, R., Torfs, T., Mohan, R., Breeschoten, A., et al. (2015). A 345 μW multi-sensor biomedical SoC with bio-impedance, 3-channel ECG, motion artifact reduction, and integrated DSP. *IEEE Journal of Solid-State Circuits*, 50(1):230–244.

Wang, J. (2002). A new method for evaluating ECG signal quality for multi-lead arrhythmia analysis. In *Computers in Cardiology Conference*, pages 85–88. IEEE.

Ward, J. and Linden, R. (2013). *Physiology at a Glance*. John Wiley & Sons, Inc.

Webster, J. (1984). Reducing motion artifacts and interference in biopotential recording. *IEEE Transactions on Biomedical Engineering*, 31(12):823–826.

Werther, T., Klotz, A., Granegger, M., Baubin, M., Feichtinger, H. G., Amann, A., and Gilly, H. (2009). Strong corruption of electrocardiograms caused by cardiopulmonary resuscitation reduces efficiency of two-channel methods for removing motion artefacts in non-shockable rhythms. *Resuscitation*, 80(11):1301–1307.

Wieben, O., Afonso, V., and Tompkins, W. (1999). Classification of premature ventricular complexes using filter bank features, induction of decision trees and a fuzzy rule-based system. *Medical and Biological Engineering and Computing*, 37(5):560–565.

Wiese, S. R., Anheier, P., Connemara, R. D., Mollner, A. T., Neils, T. F., Kahn, J. A., and Webster, J. G. (2005). Electrocardiographic motion artifact versus electrode impedance. *IEEE Transactions on Biomedical Engineering*, 52(1):136–139.

Wilson, F. N., Johnston, F. D., Macleod, A. G., and Barker, P. S. (1934). Electrocardiograms that represent the potential variations of a single electrode. *American Heart Journal*, 9(4):447–458.

Yang, Y.-S. O., Lee, W.-C., Ke, T.-C., Wei, C.-P., and Lee, C.-C. (2008). Adaptive reduction of motion artefact in wireless physiological monitoring microsystems. In *3rd International Conference on Sensing Technology*, pages 523–526. IEEE.

Yoon, S. W., Min, S. D., Yun, Y. H., Lee, S., and Lee, M. (2008). Adaptive motion artifacts reduction using 3-axis accelerometer in e-textile ECG measurement system. *Journal of Medical Systems*, 32(2):101–106.

Zhang, G., Wu, T., Wan, Z., Song, Z., Yu, M., Wang, D., Li, L., and Chen, F. (2016). A new method to detect ventricular fibrillation from CPR artifact-corrupted ECG based on the ECG alone. *Biomedical Signal Processing and Control*, 29:67–75.

Zipes, D., Festoff, B., Schaal, S., Cox, C., Sealy, W., and Wallace, A. (1968). Treatment of ventricular arrhythmia by permanent atrial pacemaker and cardiac sympathectomy. *Annals of Internal Medicine*, 68(3):591–597.

Zong, W., Moody, G., and Jiang, D. (2003). A robust open-source algorithm to detect onset and duration of QRS complexes. In *Computers in Cardiology, 2003*, pages 737–740. IEEE.